LBL-12089

Lawrence Berkeley Laboratory
UNIVERSITY OF CALIFORNIA

Materials & Molecular Research Division

LASER-INDUCED CHEMICAL REACTIONS

Ann Elizabeth Orel
(Ph.D. thesis)

December 1980

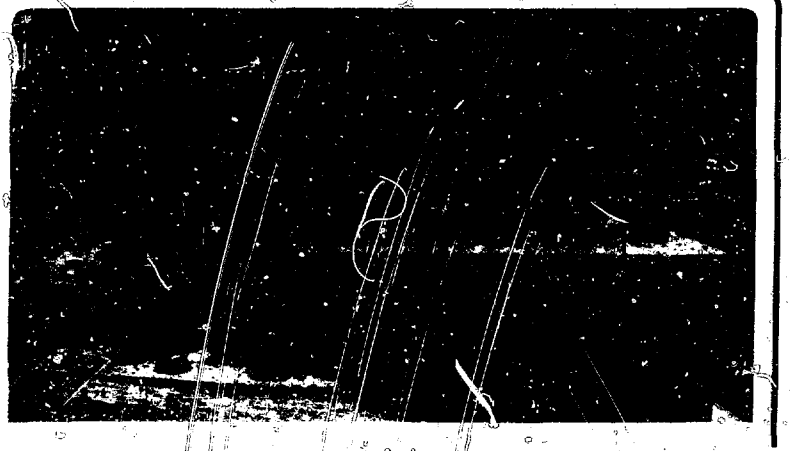

Prepared for the U.S. Department of Energy under Contract W-7405-ENG-48

Laser Induced Chemical Reactions

By

Ann Elizabeth Orel

Ph.D. Thesis

December, 1980

Department of Chemistry, and Materials and Molecular Research Division
of the Lawrence Berkeley Laboratory, University of California
Berkeley, California 94720

This work was partially supported by the Director, Office of Energy Research, Office of Basic Energy Sciences, Chemical Sciences Division of the U.S. Department of Energy under Contract Number W-7405-ENG-48.

LASER INDUCED CHEMICAL REACTIONS

ANN ELIZABETH OREL

ABSTRACT

A classical model for the interaction of laser radiation with a molecular system is derived. Within this model, all degrees of freedom, molecular, radiation and their interaction are described in a dynamically consistent framework. The classical dynamics of such a system can be calculated with the addition of the two equations of motion representing the field.

This model is used to study the enhancement of a chemical reaction via a collision induced absorption. It was found that an infrared laser will in general enhance the rate of a chemical reaction, even if the reactants are infrared inactive. Results for a illustrative analytically solvable model are presented, as well as results from classical trajectory studies on a number of systems.

The collision induced absorption spectrum in these systems can be written as the Fourier transform of a particular dipole correlation function. This is used to obtain the collision induced absorption spectrum for a state-selected, mono-energetic reactive collision system. Examples treated are a one-dimensional barrier problem, reactive and non-reactive collisions of $H + H_2$, and a modified $H + H_2$ potential energy surface which leads to a collision intermediate.

An extension of the classical model to treat laser-induced electronically non-adiabatic collision processes is constructed. The model treats all degrees of freedom, molecular, electronic and radiation, in a dynamically consistent framework within classical

mechanics. Application is made to several systems. Several interesting phenomena are discovered including a Franck-Condon-like effect causing maxima in the reaction probability at energies much below the classical threshold, laser de-enhancement of chemical reactions and an isotope effect.

In order to assess the validity of the classical model for electronically non-adiabatic process (without a laser field), a model problem involving energy transfer in a collinear atom-diatom system is studied, and the results compared to the available quantum mechanical calculation. It is found that the calculations are in qualitative agreement.

ACKNOWLEDGMENTS

I would like to thank my thesis advisor, Bill Miller, for his constant support and guidance throughout my graduate career. It was a privilege to be associated with such a creative scientist during the formative years of my career. Tom Rescigno, my other scientific guide through these years cannot be forgotten. He acted not only as a mentor but as a friend. His support of my "weekend" projects, supplying guidance and computer time with a great deal of patience, gave a much broader base to my graduate career.

Life would be impossible without my friends. Special thanks are due to Hugh and Charlie, who put up with all my ups and downs both scientific and personal, listened to my ideas, provided help, advice and a shoulder to cry on. I would also like to thank my companions in the trenches old and new, John, Richard, Boyd, Stephen, Dom, Shi Shen-Hua and Lynn who made graduate life much more bearable. Many thanks are also due to Carol Hacker, not only for her patience in typing this manuscript but for her friendship and support.

Finally I would like to thank those people most important in my life, my family, especially my parents. Their indefatigble support of my goals and aspirations continued even whese these led me far from home and away from the usual paths. They made me what I am today. It is to them that I dedicate this work.

This work was partially supported by the Director, Office of Energy Research, Office of Basic Energy Sciences, Chemical Sciences Division of the U.S. Department of Energy under Contract Number W-7405-ENG-48.

To My Parents

TABLE OF CONTENTS

Page

I. INTRODUCTION

The subject of laser interactions with molecular processes has generated great interest both experimentally and theoretically. This interest has been enhanced by the possibilities for laser-catalyzed chemical reactions, isotopic selectivity and perhaps even the determination of the transition state structure. The degree of success in this area has been limited by the extreme difficulties of the experiments involved and also the lack of simple and qualitatively accurate theoretical models that can be applied to a wide range of systems.

Classical mechanics has been widely used in studying a variety of heavy particle systems. It has been found to provide qualitatively accurate results and is relatively simple to apply. Therefore work focused on developing a classical model for the interaction of radiation with a molecular system.

This work can be divided into several broad areas. The first chapter deals with the interaction of a high power laser with a colliding molecular system. A model is developed which treats all the degrees of freedom within a classical framework. Due to the extreme simplicity of the model, which involves the addition of only two more equations of motion to the system of equations governing the classical motion of the colliding molecular system, it was possible to study a range of molecular systems including a three-dimensional A + BC type reaction. It was found that it is possible to lower the activation barrier for a chemical reaction by energy transfer from the laser field to the collision system through a collision induced

absorption, even if the original reactants are infrared inactive.

A natural extension of this work is to study the effect of the molecular dynamics on the laser field, that is the absorption and emission of photons during the collision. Since the interaction between the laser field and the colliding molecules in these systems occurs primarily in the transition state region of the potential energy surface, it is possible to obtain information about the structure of the transition state directly, in general a difficult if not impossible task. In Chapter III a simple extension of the classical model of the previous chapter is used to calculate the collision induced absorption spectra for several model systems.

The previous chapters have concentrated on the interaction of an infrared laser with a colliding molecular system, studying the effects of energy transfer to transient vibrational modes. It is also possible to study the interaction of visible/UV lasers with such systems, where the energy is now used to make transitions between different electronic potential energy surfaces. In Chapter IV, a previously derived classical model describing electronically non-adiabatic processes is combined with the classical model of the preceeding chapters to create a classical model which treats all degrees of freedom, molecular, electronic and radiation via classical mechanics. This theory is applied to several systems, LiF + H → Li + HF both collinear and three-dimensional, a model collinear reaction where the lower surface is approximately $H + H_2 \rightarrow H_2 + H$ and collinear LiF + D → Li + DF.

Finally in Chapter V a study is made of vibrational energy transfer without a laser field using the classical model for electronically non-adiabatic processes. Comparison on this system can

be made to previous quantum mechanical studies and show that the model can produce qualitatively accurate results.

II. INFRARED LASER ENHANCEMENT OF CHEMICAL REACTIONS

A. Introduction

It is well-known that an infrared laser can accelerate chemical reactions by vibrationally exciting one of the reactants.[1] For example, in the reaction

$$HC\ell(v) + K \rightarrow KC\ell(v') + H$$

a laser can be tuned to the frequency which excites $HC\ell(v=0)$ to $HC\ell(v=1)$. This excited reactant reacts at a much faster rate than the unexcited species. This method of laser enhancement of chemical reactions requires that the laser be tuned to a transition present in the reactants. However in general there exists a collision induced absorption that enhances the rates of chemical reactions by effectively lowering the activation barrier, even if the laser is far from any region where the reactants absorb, or even if the reactants are infrared inactive.[2,3]

In order to gain a qualitative understanding of this phenomena, consider the simple prototype for a reaction with an activation barrier, $H+H_2$. The reactants are infrared inactive, but in the transition state region of the potential energy surface, the asymmetric stretch mode,

$$\vec{H}\cdots\overset{\downarrow}{H}\cdots\vec{H}$$

has a non-zero dipole moment which changes with this motion and hence will absorb in the infrared. Notice that the dipole moment does not vary with the displacement of the symmetric stretch,

$$\overleftarrow{H}\cdots H\cdots\vec{H}$$

and so this mode is infrared inactive. The asymmetric stretch is motion along the reaction coordinate so the system will absorb energy from the radiation field preferentially in that degree of freedom most effective in promoting the reaction, that is helping it to surmount the activation barrier. Thus the activation energy for the reaction is lowered by the presence of the infrared laser. Without the field, there are no trajectories which react at energies below the classical threshold, while in the presence of the laser field, some of these non-reactive trajectories gain sufficient energy from the field to become reactive.

This is a general phenomena since displacement of a transition state along the reaction coordinate is, in general, the least symmetric displacement[4] and will therefore always be infrared active. It is also clear, however, that the phenomena requires very intense radiation fields (lasers) since the system is in the transition state region of the potential energy surface for only a short period of time, that is the "concentration of transition states" is small.

In addition to interest in this process for the obvious reason of being able to accelerate chemical reactions, it is also interesting because it allows one in effect to "see" (i.e., to interact with) the reactive system in the transition state region itself. In normal scattering experiments one can observe the system only before and after complete collisions. This collision induced absorption is thus the closest in principle that one can come to infrared spectroscopy of a transition state.

In the next section a classical model for the interaction of laser radiation with molecular systems is introduced. In this model, the

entire system molecules, field and their interaction is treated on a dynamically consistent framework, invoking the same approximation (classical mechanics) for both.[5] It is thus possible to use classical trajectories to describe the system with the extension into three-dimensional A + BC systems, an area almost impossible to treat quantum mechanically relatively simple to treat.

Section C presents a simplified one-dimensional model of the phenomenon that is analytically solvable. This gives a qualitative indication of the nature and order of the magnitude of the effect, i.e., how much the activation energy of a reaction is expected to be lowered by the radiation field. The results of classical trajectory calculations, including the laser field, for the reactions

$$X + H_2 \rightleftarrows HX + H \quad ,$$

for X = H, F, Cℓ are presented in Section D. The qualitative behavior predicted by the 1-dimensional model of Section C is seen to be borne out by these results.

In closing this Introduction it should be noted that collision induced absorption is a well-known and much studied phenomenon in itself, e.g., in mixed rare gases.[6] In the present chapter our interest is not so much in the absorption spectrum but rather in how the absorption affects the collision dynamics, e.g., by changing non-reactive trajectories into reactive ones. Also, there has been considerable interest in the effect of visible lasers on molecular collision processes;[7] this of course involves electronic excitation and thus requires the existence of appropriate electronically excited potential energy surfaces.

B. The Classical Model

First consider the quantum mechanical Hamiltonian for the system in the presence of a single mode radiation field. The extension to an arbitrary number of modes is straightforward. The Hamiltonian is[8,9]

$$H = H_{MOL} + H_{RAD} + H_{INT} \tag{2.1}$$

where H_{MOL} is the Hamiltonian of the isolated molecular system, H_{RAD} is the Hamiltonian of the radiation field and H_{INT} describes their interaction. Using second quantization

$$H_{RAD} = \hbar \omega a^{\dagger} a \tag{2.2}$$

where $a^{\dagger}$,a are the creation and annihilation operators of the photon field, and ω is the frequency of the field. Within the dipole approximation

$$H_{INT} = -\vec{\mu}(\underset{\sim}{x})\cdot\vec{E} \tag{2.3}$$

where $\vec{\mu}(\underset{\sim}{x})$ is the dipole moment of the molecular system as a function of the molecular coordinates $\underset{\sim}{x}$ and $\vec{E}$ is the electric field,

$$\vec{E} = i\sqrt{\frac{2\pi\hbar\omega}{V}}\ (a^{\dagger}-a)\hat{\epsilon} \tag{2.4}$$

where $\hat{\epsilon}$ is the polarization of the photon field and V is the volume of the radiation cavity. With these substitutions the total Hamiltonian becomes

$$H = H_{MOL}(\underset{\sim}{p},\underset{\sim}{x}) + \hbar\omega a^{\dagger}a + i\sqrt{\frac{2\pi\hbar\omega}{V}}\ (a^{\dagger}-a)\mu(\underset{\sim}{x}) \tag{2.5}$$

where $\underset{\sim}{p},\underset{\sim}{x}$ are the molecular momentum and coordinates and $\mu(\underset{\sim}{x}) = \vec{\mu}(\underset{\sim}{x})\cdot\hat{\epsilon}$

In order to better illustrate the classical limit, replace the operators **a** and $a^{\dagger}$ by **P** and **X** where,

$$P = \sqrt{\frac{\hbar\omega}{2}}\,(a+a^{\dagger}) \tag{2.6a}$$

$$X = \sqrt{\frac{\hbar}{2\omega}}\,i(a-a^{\dagger}) \tag{2.6b}$$

so the Hamiltonian becomes[10]

$$H(\underset{\sim}{p},\underset{\sim}{x},P,X) = H_{MOL}(\underset{\sim}{p},\underset{\sim}{x}) + \frac{1}{2}P^2 + \frac{1}{2}\omega^2 x^2 - \sqrt{\frac{4\pi\omega^2}{V}}\;\mu(\underset{\sim}{x})X \tag{2.7}$$

Notice that the Hamiltonian has the form of an oscillator coupled by a forcing term to the molecular system through the dipole moment. Since the "oscillator" (the field) is in a state described by large quantum numbers (a large number of photons) a classical approximation should be valid. Take the classical limit so that the operators, p,x,P,X become the classical variables and H(p,x,P,X) becomes the classical Hamiltonian function. The equations of motion for the system are,

$$\dot{\underset{\sim}{x}} = \frac{\partial H}{\partial \underset{\sim}{p}} = \underset{\sim}{p}/m \tag{2.8a}$$

$$\dot{\underset{\sim}{p}} = -\frac{\partial H}{\partial \underset{\sim}{x}} = -\frac{\partial V}{\partial \underset{\sim}{x}} + \sqrt{\frac{4\pi\omega^2}{V}}\;X\;\frac{\partial \mu(\underset{\sim}{x})}{\partial \underset{\sim}{x}} \tag{2.8b}$$

$$\dot{X} = \frac{\partial H}{\partial P} = P \tag{2.8c}$$

$$\dot{P} = -\frac{\partial H}{\partial X} = -\omega^2 X + \sqrt{\frac{4\pi\omega^2}{V}}\ \underset{\sim}{\mu}(\underset{\sim}{x}) \tag{2.8d}$$

Since the Hamiltonian is not an explicit function of time, the total energy of the system is conserved. Classical trajectories can be integrated for the colliding system in the presence of the field through the addition of only two more equations of motion.

It is possible to manipulate Eq. (2.8) to eliminate the field variables. First combine (2.8c) and (2.8d) to eliminate P which yields

$$\ddot{X}(t) + \omega^2 X(t) = \sqrt{\frac{4\pi\omega^2}{V}}\ \underset{\sim}{\mu}(\underset{\sim}{x}(t)) \tag{2.9}$$

This is a linear inhomogeneous equation with solution

$$X(t) = X_0(t) + \sqrt{\frac{4\pi\omega^2}{V}} \int_{t_1}^{t} dt' \frac{\sin(\omega(t-t'))}{\omega}\ \underset{\sim}{\mu}(\underset{\sim}{x}(t')) \tag{2.10}$$

where

$$X_0(t) = \sqrt{\frac{2N_1\hbar}{\omega}}\ \sin(\omega(t-t')+Q_1) \tag{2.11}$$

the solution to the homogeneous equation where (N_1,Q_1) are the values of the field action-angle variables at t_1 the initial time. (N_1,Q_1) are defined by[11]

$$X = \sqrt{\frac{2\hbar N}{\omega}}\ \sin Q \tag{2.12a}$$

$$P = \sqrt{2\hbar\omega N}\ \cos Q \tag{2.12b}$$

Using Eq. (2.10), a closed form expression for $(\underset{\sim}{p},\underset{\sim}{x})$, the molecular

variables can be derived,

$$\dot{\underset{\sim}{x}}(t) = \underset{\sim}{p}/m \tag{2.13a}$$

$$\dot{\underset{\sim}{p}}(t) = -\frac{\partial V(\underset{\sim}{x})}{\partial \underset{\sim}{x}} + \sqrt{\frac{8\pi\hbar\omega N_1}{V}}\,\frac{\partial \mu(\underset{\sim}{x})}{\partial \underset{\sim}{x}}\,\sin(\omega(t-t_1)+Q_1) \tag{2.13b}$$

$$+\frac{4\pi\omega^2}{V}\,\frac{\partial \mu(\underset{\sim}{x})}{\partial \underset{\sim}{x}}\int_{t_1}^{t} dt'\,\frac{\sin(\omega(t-t'))}{\omega}\,\mu(\underset{\sim}{x}(t'))$$

This expression is exact. It is possible to apply perturbation theory to this expression. To first order in $V^{-1/2}$, $\underset{\sim}{x}(t)$ is given by

$$\underset{\sim}{x}(t) = \underset{\sim}{x}_0(t) + \Delta\underset{\sim}{x}(t) + O(V^{-1}) \tag{2.14}$$

where

$$m\ddot{\underset{\sim}{x}}_0(t) + \frac{\partial V(\underset{\sim}{x}_0)}{\partial \underset{\sim}{x}_0} = 0 \tag{2.15}$$

(Thus $\underset{\sim}{x}_0(t)$ is the field free trajectory) and

$$\left[\frac{md^2}{dt^2} + \frac{\partial^2 V(\underset{\sim}{x}_0)}{\partial \underset{\sim}{x}_0^{\,2}}\right]\Delta\underset{\sim}{x}(t) = \sqrt{\frac{8\pi\hbar\omega N_1}{V}}\,\frac{\partial \mu(\underset{\sim}{x}_0(t))}{\partial \underset{\sim}{x}_0}\,\sin(\omega(t-t_1)+Q_1) \tag{2.16}$$

The initial conditions are

$$\underset{\sim}{x}_0(t_1) = x_1 \;;\; \dot{\underset{\sim}{x}}_0(t_1) = \underset{\sim}{p}_1/m \tag{2.17a}$$

$$\Delta\underset{\sim}{x}(t_1) = \Delta\dot{\underset{\sim}{x}}(t_1) = 0 \tag{2.17b}$$

Using these initial conditions Eq. (2.16) can be solved yielding the following expression[5] $\Delta\underset{\sim}{x}(t)$,

$$\Delta\underset{\sim}{x}(t) = \sqrt{\frac{8\pi\hbar\omega N_1}{V}} \left(\frac{\partial \underset{\sim}{x}_0(t)}{\partial \underset{\sim}{p}_1} \cdot \frac{\partial}{\partial \underset{\sim}{x}_1} - \frac{\partial \underset{\sim}{x}_0(t)}{\partial \underset{\sim}{x}_1} \frac{\partial}{\partial \underset{\sim}{p}_1}\right) \cdot$$

$$\int_{t_1}^{\infty} dt' \; \mu(\underset{\sim}{x}_0(t')) \; \sin(\omega(t'-t)+\varphi_1) \qquad (2.18)$$

where $\underset{\sim}{x}_0(t) \equiv \underset{\sim}{x}_0(t;\underset{\sim}{x}_1,\underset{\sim}{p}_1)$, the field free trajectory as a function of its initial conditions.

Thus it is possible to describe the interaction of a colliding molecular system and a laser field within a dynamically consistent, classical framework. Specific applications of the theory are described in the following sections.

C. A One-Dimensional Model

To obtain a simple analytic solution to serve as a qualitative guide to more quantitative calculations, we carry out in this section a calculation for the simplest possible version of the process we are describing. We thus assume for the present (1) that the potential energy surface is separable in the region of the transition state, (2) that only motion along the reaction coordinate is optically active, and (3) that the potential barrier in the reaction coordinate is parabolic. A further approximation is (4) that the effect of the radiation field of the motion along the reaction coordinate is treated by lowest order perturbation theory. The calculation is carried out, as are the numerical calculations reported in the next section, within the framework of the classical theory developed to treat the interaction of molecular systems with electromagnetic radiation which was described in the previous section.

Letting x denote the coordinate for motion along the reactive direction, consider a classical trajectory beginning at x_1 (cf Figure 1) at t = 0, with initial momentum p_1 ($x_1 < 0$ and $p_1 > 0$). The potential energy barrier V(x) is parabolic,

$$V(x) = -\frac{1}{2} m\omega_b^2 x^2 \quad , \tag{2.19}$$

so that the initial energy in this degree of freedom, E_1, is

$$E_1 = \frac{p_1^2}{2m} - \frac{1}{2} m\omega_b^2 x_1^2 \quad . \tag{2.20}$$

If $E_1 < 0$, as shown in Figure 1, then the field-free trajectory will clearly be non-reactive.

N_1 and Q_1 are the initial quantum number and phase of the radiation field, and we first determine the trajectory $x(t;x_1,p_1,N_1,Q_1)$, noting that it depends on the various initial conditions. According to the perturbation result obtained in the previous chapter, x(t) is given through first order in the interaction between molecule and radiation field by

$$x(t) = x_0(t) + \Delta x(t) \quad , \tag{2.21}$$

where $x_0(t)$ is the field-free trajectory, which in this case is

$$x_0(t) = x_1 \cosh(\omega_b t) + \frac{p_1}{m\omega_b} \sinh(\omega_b t) \quad , \tag{2.22}$$

and where $\Delta x(t)$ is the correction caused by the radiation field:

$$\Delta x(t) = \sqrt{\frac{8\pi\hbar\omega N_1}{V}} \int_0^t dt' \left[\frac{\partial x_0(t;x_1,p_1)}{\partial p_1} \frac{\partial x_0(t';x_1,p_1)}{\partial x_1} - \frac{\partial x_0(t;x_1,p_1)}{\partial x_1} \frac{\partial x_0(t';x_1,p_1)}{\partial p_1} \right] \mu'(x_0(t')) \sin(\omega t' + Q_1); \tag{2.23}$$

$\mu(x)$ is the dipole moment of the molecular system as a function of x. Utilizing Eq. (2.22), Eq. (2.23) becomes

$$\Delta x(t) = \sqrt{\frac{8\pi\hbar\omega N_1}{V}} (m\omega_b)^{-1} \int_0^t dt' \, \mu'(x_0(t')) \sinh[\omega_b(t-t')] \sin(\omega t' + Q_1) . \tag{2.24}$$

To determine whether the trajectory is reactive or not, we consider the limit $t \to +\infty$ to see if $x(t\to\infty) \to +\infty$ (reactive) or $-\infty$ (non-reactive). Eqs. (2.22) and (2.24) show that as $t \to +\infty$,

$$x(t) \equiv x_0(t) + \Delta x(t)$$

$$\sim \frac{1}{2} e^{\omega_b t} \left[x_1 + \frac{p_1}{m\omega_b} + \sqrt{\frac{8\pi\hbar\omega N_1}{V}} (m\omega_b)^{-1} \int_0^\infty dt' \, \mu'(x_0(t')) e^{-\omega_b t'} \sin(\omega t' + Q_1) \right] \tag{2.25}$$

To simplify matters further we also assume that the dipole derivative is constant, $\mu'(x) = \mu'$, so that

$$\int_0^\infty dt' \, \mu'(x_0(t') \, e^{-\omega_b t} \sin(\omega t' + Q_1)$$

$$= \frac{\mu'[\omega\cos Q_1 + \omega_b \sin Q_1]}{\omega^2 + \omega_b^2} , \tag{2.26}$$

and take x_1 large enough so that

$$x_1 + \frac{p_1}{m\omega_b} = x_1 + (2mE_1 + m^2\omega_b^2 x_1^2)^{1/2}/(m\omega_b)$$

$$\simeq E_1/(m\omega_b^2|x_1|) \quad . \tag{2.27}$$

Eq. (2.25), with Eq. (2.26), then implies that the trajectory is reactive or not depending on whether the following quantity is positive or negative:

$$\frac{E_1}{m\omega_b^2|x_1|} \div \sqrt{\frac{8\pi\hbar\omega N_1}{V}}\ \frac{\mu'}{m\omega_b}\ \frac{(\omega\cos Q_1 + \omega_b \sin Q_1)}{\omega^2 + \omega_b^2} \quad . \tag{2.28}$$

The <u>characteristic function for reaction</u> $\chi_R(N_1,Q_1;E_1)$, which is 1 for reactive trajectories and 0 for non-reactive ones, is thus given by

$$\chi_R(N_1,Q_1;E_1) = h[E_1 + \frac{\hbar\omega_R\omega_b}{\omega^2+\omega_b^2}(\omega\cos Q_1 + \omega_b \sin Q_1)] \quad , \tag{2.29}$$

where h( ) is the usual step-function,

$$h(z) = \begin{cases} 1, & z > 0 \\ 0, & z < 0 \end{cases} \quad ,$$

and where ω_R is the Rabi frequency for the transition,

$$\hbar\omega_R \equiv \sqrt{\frac{8\pi\hbar\omega N_1}{V}}\ |\mu' x_1| \quad . \tag{2.30}$$

The net reaction probability is obtained by averaging χ_R over the initial phase of the field,

$$P_R(N_1,E_1) = (2\pi)^{-1}\int_0^{2\pi} dQ_1\ \chi_R(N_1,Q_1;E_1) \quad , \tag{2.31}$$

and it is easy to show that with χ_R given by Eq. (2.29) the result is

$$P_R(N_1,E_1) = \frac{1}{2} + \sin^{-1}(E_1/E_{th})/\pi \quad , \tag{2.32}$$

where E_{th}, the threshold for reaction, is given by

$$E_{th} = -\hbar\omega_R(1 + \omega^2/\omega^2_b)^{-1/2} \quad . \tag{2.33}$$

Equations (2.32) and (2.33) are the principle results of this model calculation, and they should be regarded as qualitative, order-of-magnitude indicators. Figure 2 shows the reaction probability of Eq. (2.32) as a function of energy E_1, compared to the field-free result. The important feature is that the threshold for the reaction has been depressed by the presence of the radiation field. Eq. (2.33) shows that the amount by which the threshold energy is lowered is roughly $\hbar\omega_R$.

The numerical classical trajectory calculations described in the next section also show the qualitative behavior described by Eqs. (2.32) and (2.33).

The dependence of this absorption on the frequency of the laser is also easy to understand qualitatively within the framework of this one-dimensional picture. For a reactive trajectory, i.e., one that passes over the barrier in Figure 1, the time dependence of the molecular dipole moment will be of the form sketched in Figure 3a. (This would be the case, for example, for the $H + H_2 \rightarrow H_2 + H$ reaction.) In the one photon perturbative limit the absorption coefficient, i.e., the probability of the system absorbing a photon, is proportional to the square modulus of the Fourier transform of $\mu(t)$:

$$I(\omega) \propto \left| \int_{-\infty}^{\infty} dt\ e^{i\omega t}\ \mu(t) \right|^2 \quad . \tag{2.34}$$

Suppose, for example,

$$\mu(x) = \mu' \times \exp(-\tfrac{1}{2}\, x^2/a^2) \tag{2.35}$$

and

$$x(t) = vt \quad . \tag{2.36}$$

Eq. (2.34) then gives

$$I(\omega) \propto \omega^2\ \exp(-\omega^2 a^2/v^2) \quad , \tag{2.37}$$

which is sketched in Figure 3b. The probability of absorption is largest in this case for

$$\omega = v/a \quad ; \tag{2.38}$$

frequencies above or below this value are not as effective in promoting the reactive, and this optimum laser frequency is seen to vary monotonically with the collision energy.

D. Classical Trajectory Calculations

To obtain a more quantitatively reliable characterization of how this collision induced absorption enhances the rate of reactions, we have carried out classical trajectory calculations within the framework of the theoretical model developed in the previous section. In this model the molecular degrees of freedom, and also the radiation field--approximated as a single mode laser--are treated by classical mechanics, i.e., by numerically integrating Hamilton's equations for

the complete system, molecules plus radiation field.[5]

For the case of a collinear A + BC collision in a single mode radiation field, the classical Hamiltonian for the complete system is

$$H(p_R,R,p_r,r,p_X,X) = \frac{p_R^2}{2\mu} + \frac{p_r^2}{2m} + \frac{p_X^2}{2}$$

$$+ V(r,R) + \frac{1}{2}\omega^2 X^2 - \sqrt{\frac{4\pi\omega^2}{V}}\,\mu(r,R)X \quad , \qquad (2.39)$$

where (R,p_R), (r,p_r), and (X,p_X) are the coordinates and momenta for the translation of A relative to the center of mass of BC, the relative vibration of B-C, and the radiation field, respectively. μ and m are the corresponding reduced masses, ω is the frequency of the laser, V the volume of the radiation cavity, $\mu(r,R)$ is the dipole moment of the A-B-C system as a function of its configuration, and $V(r,R)$ is the field-free potential energy surface for the A-B-C system. (For the three-dimensional case $\mu(r,R)$ is replaced by $\vec{\mu}(\vec{r},\vec{R})\cdot\hat{\epsilon}$, where $\vec{\mu}$ is the dipole moment vector of the molecular system and $\hat{\epsilon}$ is the polarization vector of the radiation field.) One sees that the radiation field enters in this model as simply one additional mechanical degree of freedom, a harmonic oscillator, that is coupled to the molecular degrees of freedom. It is convenient to replace the field variables (X,p_X) by the action-angle variables (N,Q), defined in the usual manner,[11]

$$X = \sqrt{\frac{2\hbar N}{\omega}}\,\sin Q \qquad (2.40a)$$

$$P = \sqrt{2\hbar\omega N}\cos Q \quad , \qquad (2.40b)$$

and the Hamiltonian then becomes

$$H(p_R,R,p_r,r,N,Q) = \frac{p_R^2}{2\mu} + \frac{p_r^2}{2m} + V(r,R) + \hbar\omega(N+\tfrac{1}{2})$$

$$-\sqrt{\frac{8\pi\hbar\omega N}{V}}\ \mu(r,R)\ \sin Q \quad . \tag{2.41}$$

N is the quantum number of the radiation field oscillator, i.e., the number of photons in the field, and Q is the phase of the field.

The initial conditions for the classical trajectories are

$$R(t_1) = \text{large } (>> 0)$$

$$p_R(t_1) = -\sqrt{2\mu E_1}$$

$$N(t_1) = N_1$$

$$Q(t_1) = Q_1$$

$$r(t_1) = r(n_1,q_1)$$

$$p_r(t_1) = p(n_1,q_1) \quad , \tag{2.42}$$

where r(n,q) and p(n,q) are the algebraic functions expressing the vibrational variables (r,p_r) in terms of the vibrational action-angle variables (n,q). (For the present examples the vibrational potential of the isolated BC molecules is a Morse potential so that the functions r(n,q) and p(n,q) are those given before.)[12] E_1 is the initial translational energy, and the quantum numbers n_1 and N_1 are integers, the initial vibrational state of BC and the initial number of photons in the radiation field, respectively.

To carry out the usual quasi-classical type calculation[13] it is useful to define the characteristic function for reaction $\chi_R(q_1,Q_1,n_1,N_1;E_1)$, which is 1 if the trajectory with these initial conditions is reactive, and 0 if it is non-reactive. The total reaction probability from the initial vibrational state n_1, with initial translational energy E_1, and with N_1 photons initially in the radiation field, is then given in the quasiclassical framework by

$$P_R(n_1,N_1;E_1) = (2\pi)^{-2} \int_0^{2\pi} dq_1 \int_0^{2\pi} dQ_1 \, \chi_R(q_1,Q_1,n_1,N_1;E_1) \quad . \quad (2.43)$$

The above discussion is modified in a reasonably obvious fashion to treat the three-dimensional version of an A + BC collision process.

a. $\underline{H + H_2 \rightarrow H_2 + H}$

Although this reaction is not of great interest in itself, it is the simplest prototype chemical reaction, and since it is so well-characterized and since the reactants are infrared inactive, it is a good example to illustrate this collisionally induced absorption.

The Porter-Karplus[14] potential energy surface was employed in the trajectory calculations reported here, and the following dipole moment function was used:

$$\mu(r,R) = s \, \mathrm{sech}^2(s) \quad , \quad (2.44)$$

where

$$s = \frac{3}{2} r - R \quad ;$$

s is the asymmetric stretch coordinate at the saddle point of the

potential energy surface. Although not quantitative, this dipole moment function is qualitatively correct, and an overall multiplicative constant is absorbed in the definition of ω_R. Three field strengths were studied, corresponding to $\hbar\omega_R$ = 0.001, 0.01, and 0.1 eV. At the lowest value little effect is observable, but for $\hbar\omega_R$ = .01 eV the reactive threshold was lowered as expected and as explained by the model in Section C. For the largest laser power ($\hbar\omega_R$ = 0.1 eV) the effect is most significant, and these results are shown in Figure 4.

The variation of threshold lowering with laser frequency is summarized in Table I. Since the dipole moment is similar to that shown in Figure 3a, it was expected that the absorption would be similar to that of Figure 3b and that the effect would thus peak at some finite laser frequency. This is observable in Table I, the optimum laser frequency being $\sim$ 500 cm^{-1}.

b. $\underline{F + H_2 \rightleftarrows HF + H}$

This system has a very asymmetric barrier. In the forward direction it is enhanced by translational energy, and in the backward direction HF will not react collinearly unless excited to the v=2 vibrational state.

Polanyi's SE1 surface,[15] a semi-empirical modified LEPS (London-Eyring-Polanyi-Sato) potential surface, was used in this calculation, the parameters for which are summarized in Table II. The dipole moment function for F-H-H was approximated as the sum of the two individual H-F dipole moments, where the H-F moment as a function of internuclear distance is the theoretical result of Lie[16] which was fit to the form

$$\mu(r) = e^{-\alpha r} \sum_{n=0}^{5} c_n r^n \quad ; \qquad (2.45)$$

the parameters of this fit are given in Table III.

The collinear results for $F + H_2(v=0) \rightarrow HF + H$ are shown in Figure 5 for $\hbar\omega_R = 0.1$ eV, corresponding to a laser power of ~ 30 gigawatts/cm^2; they are seen to be qualitatively similar to $H + H_2 \rightarrow H_2 + H$ above. Similar results for the reverse reaction, $H + HF(v) \rightarrow H_2 + F$, are shown in Figure 6 for v=2. There is no reaction, with or without the laser, for v=0,1, and for v=3 the increased vibrational energy damps out the laser effect.

In contrast to the $H + H_2$ reaction, the variation of the dipole moment with time for $F + H_2 \rightleftarrows HF + H$ behaves qualitatively as a smooth step-function, i.e., it rises from zero to a finite value along the reaction coordinate, unlike that in Figure (3a). In this case its Fourier transform is a monotonically decreasing function of frequency ω; i.e., $I(\omega)$ increases as ω decreases. In this case one thus expects the effect of the collision induced absorption to increase monotonically with decreasing laser frequency. The dependence of the threshold lowering on laser frequency for this reaction (cf. Table I) does indeed show this behavior.

c. $Cl + H_2 \rightleftarrows HCl + H$

The parameters for the modified LEPS potential surface used in the calculation are summarized in Table II.[17] The dipole moment function of HCl was fit to the same general shape as the HF dipole moment but scaled so that the correct value was obtained for both the dipole moment and dipole moment derivative at the equilibrium bond

distance. The parameters are summarized in Table III.

The results for collinear $C\ell + H_2(v=0) \rightarrow HC\ell + H$ are shown in Figure 7 for $\hbar\omega_R = 0.1$ eV and for 0.01 eV, and the effect of varying the laser frequency is summarized in Table I. Results for the reverse reaction, $H + HC\ell(v=0) \rightarrow H_2 + C\ell$, are shown in Figure 8 for $\hbar\omega_R = 0.1$ eV. The overall behavior is similar to that of $F + H_2$ discussed above.

Note however that the effect in this case is much larger, with a noticeable lowering occuring even at a laser field strength of 0.01 eV. This can be explained simply in terms of a mass effect. The threshold lowering is dependent not only on the field strength, but also on the time the system spends in the interaction region. In the case of chlorine, for a given translational energy, the system spends a longer period of time near the transition region, hence the effect is larger.

d. $C\ell + H_2 \rightarrow HC\ell + H$ (3 dimensions)

Finally, three dimensional trajectory calculations were carried out for $C\ell + H_2(v=0, j=0) \rightarrow HC\ell + H$ for $\hbar\omega_R = 0.1$ eV. The interest here is to see if the effect of threshold lowering is diminished by the additional degrees of freedom present for the three dimensional collision system. The potential surface and dipole moment function are the same as those used above for the collinear calculation.

Another interesting feature of the three-dimensional system is the effect of polarization of the laser beam. One thus imagines a molecular beam experiment with beams of $C\ell$ and of H_2 crossed at right angles, and with the laser beam perpendicular to the two of them;

i.e., the three beams form the edge of a cube. The electric field vector of the laser beam, i.e., the polarization vector, then lies in the plane of the two molecular beams, and we consider the two canonical cases that the polarization vector is parallel to the initial relative velocity vector of Cℓ and H_2 or that it is perpendicular to the initial relative velocity vector.

If the reaction proceeds primarily through nearly collinear geometries and is limited to small impact parameters, then one expects the parallel polarization to be most effective in enhancing the reaction since the dipole moment function $\vec{\mu}(\vec{r},\vec{R})$ would then be approximately parallel to the polarization vector $\hat{\epsilon}$, so that $|\hat{\epsilon}\cdot\vec{\mu}|$ has its largest value. Conversely, perpendicular polarization would cause $\vec{\mu}$ to be approximately perpendicular to $\hat{\epsilon}$, so that $|\hat{\epsilon}\cdot\vec{\mu}| \sim 0$.

Figure 9 shows the reactive cross section as a function of initial translation energy for the field-free case and for parallel and perpendicular polarizations. One sees that parallel polarization is indeed more effective--perpendicular polarization gives almost no effect at all-- and one sees that the effect is not at all diminished in three dimensions.

The frequency dependence of the threshold lowering is given in Table I and is similar to the above results for the collinear case.

E. Conclusion

The classical trajectory calculations for the various A + BC → AB + C reactions described in Section D give a good characterization of how this collision induced absorption effects the reaction probability, most significantly by lowering the activation energy

for reaction. The three-dimensional calculations for $C\ell + H_2 \rightarrow HC\ell + H$ showed that the effect is not significantly diminished by the additional degrees of freedom present in the three-dimensional case, and that the polarization of the laser field can be a very interesting parameter of the process.

In these calculations the field strengths necessary to produce noticeable effects were disappointingly large. However the value of the calculations is in indicating that such an effect is indeed possible but the ideal system for such an observation were not the simple systems which were studied here. Such a system requires a very large dipole moment in the transition state region, as well as (for the largest possible effect), a system which spends several vibrational periods in the transition state region, that is one that forms a collision complex. If this does occur, other properties of the system, in some ways more interesting than the simple effects described here, can be studied. A system of this type is discussed in the next chapter.

III. COLLISION INDUCED ABSORPTION SPECTRA

A. Introduction

In the previous chapter it was shown that a high power infrared laser could influence the rate of a chemical reaction.[2,3] That study concentrated on the influence of the laser field on the molecular dynamics. However, the converse effect, that is the effect of the molecular dynamics on the laser field in the form of emission and absorption of photons, is in some ways much more interesting. This chapter will study the collision induced absorption (CIA) spectrum of the reacting system.[18] This is the analog of the well-known non-reactive CIA process for a reacting system.[4]

As noted previously, the system gains and loses energy (thereby absorbing or emitting photons) only in the region of the transition state. Thus it should be possible to observe directly the molecular motion in the transition state region of the potential energy surface, to perform spectroscopy of the transition state itself. This is in contrast to the majority of conventional scattering experiments which prepare the system in a given state before reaction and then observe the products after the reaction is complete, gaining only indirect information as to the transition state structure.

This method would also probe the reaction dynamics. Qualitatively, if the reaction was direct, the collision induced absorption spectrum should be broad with differences perhaps between reactive and non-reactive systems. If a long-lived collision complex was formed during the reaction, the spectrum would have structure. Information

as to the lifetimes and structure of the complex could be abstracted by considering the widths and positions of the absorption bands.

In this chapter two special features which arise in the study of collision induced absorption for reactive systems are considered; the differences due to reactive vs. non-reactive trajectories, and the additional structure which appears in the CIA spectrum when a collision complex is formed. Section B derives the theoretical basis for the study of collision induced absorption in a completely classical framework, building on the results of the previous chapter. In order to gain a qualitative feel for the differences between CIA spectra for reactive vs. non-reactive processes, Section C treats the model problem of a particle passing over (reacting) or being reflected by (not reacting) a one-dimensional barrier. In Section D a more realistic model, collinear $H + H_2 \rightarrow H_2 + H$ is studied and found to exhibit many of the features which were present in the one-dimensional model of Section C. Finally, Section E treats a modified $H + H_2$ like system where a small potential well is introduced at the saddle point of the potential energy surface. This causes some trajectories to form short-lived collision complexes which cause additional features in the CIA spectrum.

B. Theory

In the previous chapter it was shown that

$$X(t) = X_0(t) + \sqrt{\frac{4\pi\omega^2}{V}} \int_{t_1}^{t} dt' \, \frac{\sin(\omega(t-t'))}{\omega} \, \mu(\underset{\sim}{x}(t')) \qquad (3.1)$$

Using the equations of motion and the definitions of N and Q,[11]

$$X = \sqrt{\frac{2\hbar N}{\omega}} \sin Q \tag{3.2a}$$

$$P = \sqrt{2N\hbar\omega} \cos Q \tag{3.2b}$$

it is possible to determine the photon number N at any time t_2 as

$$\hbar\omega N(t_2) = \frac{1}{2}\dot{X}(t_2)^2 + \frac{1}{2}\omega^2 X(t_2)^2 \tag{3.3}$$

Using the expressions for X(t) and $\dot{X}(t)$ yields[5]

$$N_2\hbar\omega = N_1\hbar\omega + \sqrt{\frac{8\pi\hbar\omega^3 N_1}{V}} \int_{t_1}^{t_2} dt\ \mu(\underset{\sim}{x}(t)) \cos(\omega(t-t_1)+Q_1)$$

$$+ \sqrt{\frac{2\pi\omega^2}{V}} \left| \int_{t_1}^{t_2} dt\ e^{-i\omega t}\ \mu(\underset{\sim}{x}(t)) \right|^2 \tag{3.4}$$

where $N_n = N(t_n)$, Q_1 is the initial phase of the field and $\underset{\sim}{x}(t)$ is the molecular trajectory determined from integrating the full equations of motion of the system. The second term which has no N_1 term present is the classical analog of spontaneous emission within this model. It has been discussed elsewhere.[5,19,20] In the present application this term is insignificant and will be ignored.

This expression for $\Delta N\hbar\omega$ is exact within this model. In the following sections this expression is used to calculation collision induced absorption spectra and to check more approximate perturbation expressions. The perturbative limit of this equation is very interesting and will also be used in this chapter.

As before the perturbation limit is taken in terms of $V^{-1/2}$ where

$$\underset{\sim}{x}(t) = \underset{\sim}{x}_0(t) + \Delta\underset{\sim}{x}(t) + O(V^{-1}) \tag{3.5}$$

and the equations for $\underset{\sim}{x}_0(t)$ and $\Delta\underset{\sim}{x}(t)$ are given in the previous chapter. (Eqs. 2.15 and 2.18). To order V^{-1}

$$\Delta N\hbar\omega = \sqrt{\frac{8\pi\hbar\omega^3 N_1}{V}} \int_{t_1}^{t_2} dt\ \mu(\underset{\sim}{x}_0(t))\ \cos(\omega(t-t_1)+Q_1)$$

$$+\sqrt{\frac{8\pi\hbar\omega^3 N_1}{V}} \int_{t_1}^{t_2} dt\ \frac{\partial\mu(\underset{\sim}{x}_0(t))}{\partial\underset{\sim}{x}_0} \cdot \Delta\underset{\sim}{x}(t)\ \cos(\omega(t-t_1)+Q_1) \tag{3.6}$$

Substituting in for $\Delta\underset{\sim}{x}(t)$ and averaging over Q_1 the initial phase of the field yields,[5]

$$\Delta N\hbar\omega = \frac{4\pi\hbar\omega^2 N_1}{V} \int_{t_1}^{t_2} dt \int_{t_1}^{t} dt' \left[\frac{\partial\mu(\underset{\sim}{x}_0(t))}{\partial\underset{\sim}{p}_1} \cdot \frac{\partial\mu(\underset{\sim}{x}_0(t'))}{\partial\underset{\sim}{x}_1} - \frac{\partial\mu(\underset{\sim}{x}_0(t))}{\partial\underset{\sim}{x}_1} \cdot \frac{\partial\mu(\underset{\sim}{x}_0(t'))}{\partial\underset{\sim}{p}_1}\right]$$

$$\sin(\omega t'-\omega t) \tag{3.7}$$

Therefore it is possible to compute the energy change of the colliding molecular system (the change in the energy of the field) and hence the absorption and emission properties of the system, by integrating classical trajectories with the two additional equations of motion for the field. Several examples of this technique are given in the following sections.

C. A One Dimensional Barrier

This calculation was carried out, as were the calculations presented in later sections, within the framework of the classical theory developed in the previous chapters to treat the interaction

of molecular systems with electromagnetic radiation.[5] The usefulness of this classical model is that it provides a dynamically consistent description of the molecular system and of the radiation field and permits essentially exact (i.e., non-perturbative) calculations to be carried out. (Because the molecular dynamics is that of reactive scattering, a completely quantum mechanical treatment would be prohibitive.) Quantum effects could in principle be incorporated via classical S-matrix theory,[21] although the nature of such effects is well understood and are not expected to change any of the essential features of the results.

As shown in the previous section the change in the energy of the radiation field during the collision is given by

$$(N_2-N_1)\hbar\omega = \Delta N\hbar\omega =$$

$$\sqrt{\frac{8\pi\hbar\omega^3 N_1}{V}} \int_{t_1}^{t_2} dt\ \mu[\underset{\sim}{x}(t)]\ \cos[\omega(t-t_1) + Q_1] \qquad (3.8)$$

where N_1, Q_1 are the initial number of photons and initial phase of the field, N_2 is the final number of photons, $\underset{\sim}{x}(t)$ is the molecular trajectory, $\mu[\underset{\sim}{x}(t)]$ is the component of the dipole moment along the polarization vector of the electric field as a function of time along the trajectory, ω is the frequency of the laser, V is the volume of the radiation cavity and t_1, t_2 are the initial and final times, respectively.

Though this model allows the calculation of non-perturbative results, it is useful to consider the analytic expression obtained in the perturbative limit. If $\underset{\sim}{x}$ and $\underset{\sim}{p}$ denote the molecular coordinates

and momenta, then the fractional change in the photon energy for initial conditions $(\underset{\sim}{x}_1, \underset{\sim}{p}_1)$ is

$$F(\omega) \equiv \frac{\Delta N}{N_1} = \frac{4\pi\omega}{V} \int_{-\infty}^{\infty} dt \int_{-\infty}^{t} dt' \sin[\omega(t'-t)]$$

$$\times \left[\frac{\partial \mu(t)}{\partial \underset{\sim}{p}_1} \cdot \frac{\partial \mu(t')}{\partial \underset{\sim}{x}_1} - \frac{\partial \mu(t)}{\partial \underset{\sim}{x}_1} \cdot \frac{\partial \mu(t')}{\partial \underset{\sim}{p}_1}\right] . \qquad (3.9)$$

By introducing the transformation

$$t'-t = \Delta t$$

$$t = t \quad ,$$

Eq. (3.9) can be written

$$F(\omega) = \frac{4\pi\omega}{V} \int_0^{\infty} d(\Delta t) \sin(\omega\Delta t)\ C(\Delta t) \quad , \qquad (3.10)$$

where the correlation function $C(\Delta t)$ is

$$C(\Delta t) = \int_{-\infty}^{\infty} dt \left[\frac{\partial \mu(t)}{\partial \underset{\sim}{p}_1} \cdot \frac{\partial \mu(t-\Delta t)}{\partial \underset{\sim}{x}_1} - \frac{\partial \mu(t)}{\partial \underset{\sim}{x}_1} \cdot \frac{\partial \mu(t-\Delta t)}{\partial \underset{\sim}{p}_1}\right] . \qquad (3.11)$$

The correlation function must be averaged over the appropriate distribution of initial conditions $(\underset{\sim}{x}_1, \underset{\sim}{p}_1)$. If this were a Boltzmann distribution, then $F(\omega)$ would be proportional to the standard expression[22] for the absorption coefficient of a molecular system and would always be positive. For a state- and energy-selected collision process, however, this average is only over the angle variables conjugate to the bound degrees of freedom. For a collinear A + BC collision, for example, with a specific initial translational energy and a specific initial vibrational state of BC, the average over

initial conditions is only over the initial phase of the vibrational degree of freedom. As a consequence the averaged value $F(\omega)$ need not be positive.

To illustrate the qualitative nature of $C(\Delta t)$ and $F(\omega)$ as a function of laser frequency, a simple one-dimensional potential barrier was studied,

$$V(x) = -\frac{1}{2} m\omega_b x^2 \quad . \tag{3.12}$$

The initial energy is given by

$$E_1 = \frac{p_1^2}{2m} - \frac{1}{2} m\omega_b^2 x_1^2 \quad , \tag{3.13}$$

and the trajectory is reactive or non-reactive for $E_1 > 0$ or $E_1 < 0$, respectively; cf. Figure 1. The field-free trajectory is given by

$$x_0(t) = x_1 \cosh(\omega_b t) + \frac{p_1}{m\omega_b} \sinh(\omega_b t) \quad , \tag{3.14}$$

and dipole moment $\mu(x)$ selected for the calculation was

$$\mu(x) = x \operatorname{sech}^2 x \quad . \tag{3.15}$$

Choosing ω_b (=.001 atomic unit), m (= 1 amu) and x_1 (= -10.0 a_0, large enough that $\mu(x) \approx 0.0$) allows $C(\Delta t)$ and $F(\omega)$ to be calculated for a series of fixed initial energies E_1. Figures 10 and 11 show typical results for the case of a non-reactive (NR) trajectory (E_1 = -0.1 eV) and a reactive (R) trajectory (E_1 = 0.1 eV). For both $C(\Delta t)$ and $F(\omega)$ the NR result is very similar to conventional[6]

collision induced absorption spectra in non-reactive systems, but the R case is seen to be qualitatively different: depending on the laser frequency ω, the molecular system can either gain energy from or lose energy to the radiation field. This was also indicated in the previous chapter where, depending on the translational energy and laser frequency, the reaction probability was either increased or decreased.

D. Classical Trajectory Calculations

To obtain a more quantitatively reliable characterization of the correlation function and its corresponding collision induced absorption spectrum, classical trajectories were carried out for the collinear $H + H_2$ reaction within the framework of the theoretical model described previously. The classical Hamiltonian for the complete system, molecular system plus radiation field, is

$$H(p,r,P,R,N,Q) = \frac{p^2}{2\mu} + \frac{P^2}{2m} + V(r,R) + \hbar\omega N - \sqrt{\frac{8\pi\hbar\omega N}{V}}\,\mu(r,R)\,\sin Q \quad , \qquad (3.16)$$

and the initial conditions for the trajectories are

$$R(t_1) = \text{large}$$

$$P(t_1) = -\sqrt{2\mu E_1}$$

$$N(t_1) = N_1$$

$$Q(t_1) = Q_1$$

$$r(t_1) = r(n_1,q_1)$$

$$p(t_1) = p(n_1,q_1) \tag{3.17}$$

where $r(n_1,q_1)$, $p(n_1,q_1)$ are the algebraic functions expressing the vibrational variables (r,p) in terms of the vibrational action-angle variables (n,q). In Eq. (3.16) V(r,R) is the potential energy surface and $\mu(r,R)$ the dipole moment of the $H + H_2$ system. For the potential energy surface a modified LEPS (London-Eyring-Polanyi-Sato) function was used, the parameters of which are summarized in Table IV.[23] The dipole moment function was taken to be

$$\mu(r,R) = \mu_0 \; s \; \mathrm{sech}^2 s \quad , \tag{3.18}$$

where $s = \frac{3}{2}\, r-R$ is the asymmetric stretch coordinate at the saddle point of the potential surface. This form for the dipole moment is qualitatively correct, although there is no reason to believe that it is quantitative. Within the perturbation limit the constant μ_0 enters as simply a multiplicative constant in $C(\Delta t)$ and $F(\omega)$.

The CIA spectrum F( ) is given in an exact calculation by

$$F(\omega) = (N_1 h\omega)^{-1}\sqrt{\frac{8\pi h\omega^3 N_1}{V}}\;(2\pi)^{-2}\int_0^{2\pi} dq_1 \int_0^{2\pi} dQ_1$$

$$\times \int_{t_1}^{t_2} dt\; \mu[\underset{\sim}{x}(t)]\cos[\omega(t-t_1) + Q_1] \quad , \tag{3.19}$$

where $\underset{\sim}{x}(t)$ is the molecular trajectory determined by integrating Hamilton's equations (generated from the Hamiltonian in Eq. (3.16) with the initial conditions of Eq. (3.17)). In a perturbative calculation only the field-free trajectory is calculated. This corresponds

to the following equations of motion:

$$\dot{R} = \frac{\partial H}{\partial P} = P/\mu$$

$$\dot{P} = -\frac{\partial H}{\partial R} = -\frac{\partial V}{\partial R}$$

$$\dot{r} = \frac{\partial H}{\partial p} = p/m$$

$$\dot{p} = -\frac{\partial H}{\partial r} = -\frac{\partial V}{\partial r} \quad . \tag{3.20}$$

However since the derivatives of the dipole moment with respect to the initial conditions as a function of time are also necessary, the additional equations of motion governing the derivatives of the dynamical variables with respect to the initial conditions must also be integrated. These are[24]

$$\frac{d}{dt}\,[\underset{\approx}{R}(t)] + [\underset{\approx}{F}(t)\cdot\underset{\approx}{R}(t)] = 0 \tag{3.21}$$

where

$$\underset{\approx}{R}(t) = \begin{pmatrix} \dfrac{\partial \underset{\sim}{q}(t)}{\partial \underset{\sim}{q}_1} & \dfrac{\partial \underset{\sim}{q}(t)}{\partial \underset{\sim}{p}_1} \\ \dfrac{\partial \underset{\sim}{p}(t)}{\partial \underset{\sim}{q}_1} & \dfrac{\partial \underset{\sim}{p}(t)}{\partial \underset{\sim}{p}_1} \end{pmatrix}$$

$$\underset{\approx}{F}(t) = \begin{pmatrix} -\dfrac{\partial^2 H}{\partial \underset{\sim}{p}\partial \underset{\sim}{q}} & -\dfrac{\partial^2 H}{\partial \underset{\sim}{p}^2} \\ \dfrac{\partial^2 H}{\partial \underset{\sim}{q}^2} & \dfrac{\partial^2 H}{\partial \underset{\sim}{q}\partial \underset{\sim}{p}} \end{pmatrix}$$

where $R(t_1)$ is the unit matrix. This information allows the construction of $C(\Delta t)$ via [Eq. (3.11)], which is Fourier sine-transformed [Eq. (3.10)] to obtain $I(\omega)$. As in the exact case $C(\Delta t)$, and hence $I(\omega)$, requires an average over initial conditions, which in the case of the collinear perturbative result is just an average over the initial phase of the BC oscillator.

A typical correlation function generated by non-reactive trajectories is shown in Figure 12. (The initial vibrational state $n_1=0$, the translational energy E_1 = 0.1 eV, and all trajectories in this case are non-reactive.) The overall shape is basically the same as the NR correlation function in Figure 10 except for a superimposed high frequency oscillation. This oscillation is due to changes in the dipole moment caused by the H_2 vibrational motion relative to the incoming H [Eq. (3.18)]. The absorption spectra (calculated perturbatively) is shown in Figure 13. There are two peaks, one at low frequency due basically to translational motion and one at high frequency (at the H_2 vibrational frequency). The spectrum was also computed non-perturbatively and found to agree well with the perturbative calculation.

Figures 14 and 15 show the correlation function and corresponding absorption spectrum, respectively, which are determined from reactive trajectories of H + H_2. (In this case $n_1=0$, $E_1=0.30$ eV and 94% of the trajectories are reactive.) One again sees a high frequency oscillation in $C(\Delta t)$ which comes from vibration of H_2, and apart from this the correlation function and spectrum are similar to the reactive case of the one-dimensional model of Section III.

Referring to the absorption spectra in Figures 13 and 15, one sees that the collision system will absorb frequencies in the vicinity of the H_2 vibrational frequency. The collisional perturbation induces a dipole in H_2 and thus makes it IR active, and such an effect would exist for any collision partner. Wormer and Van Dijk,[25] for example, have recently carried out calculations for absorption in H_2 induced by collision with He atoms.

Absorption at the lower frequencies (cf. Figures 13 and 15), however, is more relevant to the process of our interest; it is related to translational motion along the reaction coordinate. It is this region of the absorption spectrum, therefore, that is most closely related to the reaction dynamics.

E. Model for a Short-Lived Collision Intermediate

To investigate the sensitivity of the correlation function and absorption spectrum to the reaction dynamics, the H + H_2 potential energy surface was modified by introducing a well at the top of the potential barrier. This causes H and H_2 to form a short-lived collision intermediate, i.e., some trajectories oscillate several times in the vicinity of the well before passing on to products (or back to reactants).

The potential surface used in the calculation was the LEPS surface described in the previous section plus an additional term V_{well}, where

$$V_{well} = c\, e^{-\alpha[(R_1-c_1)^2 + (R_2-c_2)^2]} \tag{3.22}$$

where α, c, c_1, c_2 are constants and R_1,R_2 are the interatomic distances. For this calculation, $c_1 = c_2 = 1.7574\ a_0$, $\alpha = -0.01$, which placed a gaussian well at the saddle point. The frequencies of the normal modes associated with the bottom of the well are $\omega_1 = 0.008$ and $\omega_2 = 0.015$ (atomic units).

The correlation function for this system is shown in Figure 16 for a translational energy of 0.1 eV. Due to the changes in the surface caused by the well $\sim$ 82% of the trajectories reacted, $\sim$ 37% remained in the well for one or more complete vibrations, $\sim$ 14% for two or more complete vibrations and $\sim$ 2% for three complete vibrations. Due to these effects the correlation function has more structure than in the calculation without the well, and it retains a high frequency oscillation due to the H_2 vibration.

Figure 17 shows the absorption spectrum, which also shows considerably more structure. This spectrum is essentially that of the collision complex, and one does, in fact, see peaks at ω_1 and ω_2, the harmonic frequencies related to the potential well, as well as peaks of $2\omega_1$ and $\omega_1 + \omega_2$. There are other peaks, however, which are not readily identified in terms of the harmonic frequencies. Since the potential well is shallow and very unharmonic, this is not surprising.

If the collision complex were long-lived, one would expect to see much sharper lines in the absorption spectrum. From these one could in principle determine the geometry and force constants of the collision intermediate.

F. Conclusion

We have given the basic equations (cf. Section B) which relate the CIA absorption spectrum for a state-selected, mono-energetic collision system to a particular dipole correlation function. A Boltzmann average over initial states and collision energy converts these expressions into the standard ones.[22]

The first application of these formulae (Section C) was to a particle moving in one dimension over, or being reflected by, a potential barrier. Application (in Section D) to a more realistic model of a chemical reaction, collinear $H + H_2$, showed that the qualititative behavior seen in the one-dimensional model also appears in the more realistic model.

Finally, the model treated in Section E showed how the CIA spectrum is changed when the reaction mechanism involves the formation of a collision intermediate. It is effects such as this that would make experimental observation of these spectra informative of the reaction dynamics.

IV. LASER-INDUCED NON-ADIABATIC COLLISION PROCESSES

A. Introduction

There has been considerable interest recently in how high power lasers affect molecular collision processes. Most papers on the topic have been theoretical,[2,3,5,7,18,26-31] although there have been some reports[32-36] of experiments which show these effects. Most workers, both theoretical and experimental, have dealt with the effect of visible/UV lasers, i.e., those which can cause electronic excitations, but it has been pointed out in the previous chapters that high power infrared lasers can also modify collision processes (e.g., increase rate constants for chemical reactions) without causing electronic excitation.

The purpose of this chapter, which also considers the effect of visible/UV lasers on collision phenomena, is two-fold. First, we show how a completely classical model can be constructed for such processes, i.e., one which describes the nuclear motion (translation, rotation, and vibration), electronic degrees of freedom, and the laser radiation field all by classical mechanics and thus in a dynamically consistent framework. The usefulness of this kind of approach is apparent if one wishes to describe molecular collision phenomena, e.g., atom-diatom inelastic and reactive collisions: the large number of quantum states (electronic, vibrational, rotational, and photon) involved makes quantum mechanical treatments extremely difficult and limited to special cases (e.g., collinear A + BC collision systems). With the classical model described below, on the other hand, calculations

can be carried out with standard classical trajectory methods; for A + BC collisions, for example, the only difference from the standard situation is that there are two additional classical degrees of freedom, the electronic degree of freedom and the photon degree of freedom. Quantum effects, if they are thought to be significant, can be incorporated to some extent within the "classical S-matrix" model.[21]

This classical model, which we develop in Section B, is essentially a synthesis of two earlier developments: In the previous chapters a classical model has been developed and applied for molecular collisions on <u>one</u> potential energy surface (i.e., one adiabatic electronic state) in a radiation field--i.e., a model which treats the nuclear degrees of freedom (i.e., translation, rotation, and vibration) and the photon degree of freedom by classical mechanics.[2,3,5,18] Meyer, McCurdy, and Miller[37] have developed a model for electronically non-adiabatic collision processes which treats the nuclear degree of freedom and the electronic degrees of freedom all classically. Here, therefore, we present a classical model which treats everything--nuclear degrees of freedom, electronic degrees of freedom, and the photon degrees of freedom--classically. Again, the advantage of this approach is that it is straightforward, via numerical integration of the classical equations of motion, to describe the interaction of all these degrees of freedom dynamically consistently.[30]

Section C of this chapter applys this classical model to a test problem, the reaction

$$LiF + H \rightarrow Li + HF$$

as considered by Light and Altenberger-Siczek,[29] who carried out quantum mechanical coupled-channel calculations. The interest is to see how the reaction probability is affected by a visible/UV laser which can cause electronic excitation during the collision. The results of our classical model are consistent with the quantum results, where the latter exist, but more importantly, we investigate a wider range of initial collision energies and this reveals an interesting structure in the energy dependence of the reaction probability: at energies below the threshold for reaction without the laser, the reaction probability is significantly enhanced at particular collision energies (which depend on the frequency of the laser). This effect is understood as a Franck-Condon-like effect and should pertain in general. Also in this section the additional complications involved in a full three-dimensional calculation are discussed and results presented for three dimensional LiF + H → Li + FH for a variety of field strengths and frequencies.

Finally, in the last two sections we present calculations on two other interesting phenomena. The possibility of laser inhibition of a chemical reaction is studied using a collinear model with parameters similar to $H + H_2$. This inhibition is a very large effect which can be seen at quite small laser field strengths, and which can sometimes destroy the effect of increased reaction probability on the lower state. The last section deals with the isotopic effects on reaction probability induced by the substitution of deuterium for hydrogen in the collinear reaction LiF + H.

B. The Classical Model

The classical Hamiltonian for a molecular system and a single mode radiation field has the standard form

$$H = H_{mol} + H_{rad} + H_{int} \quad , \tag{4.1}$$

where the various terms are the molecular Hamiltonian, which involves nuclear (i.e., translational, rotational, and vibrational) and electronic degrees of freedom, the Hamiltonian for the pure radiation field, and the interaction between the two, respectively. If $(\underset{\sim}{x},\underset{\sim}{p})$ denote the nuclear coordinates and momenta and (n,q) the classical action-angle variables for the electronic degrees of freedom (assuming a 2-state electronic system), then the Meyer-McCurdy-Miller[37] theory gives the molecular Hamiltonian as

$$H_{mol}(\underset{\sim}{p},\underset{\sim}{x},n,q) = \frac{\underset{\sim}{p}^2}{2m} + (1-n)H_{00}(\underset{\sim}{x}) + H_{11}(\underset{\sim}{x}) + 2\sqrt{n(1-n)}\, H_{01}(\underset{\sim}{x})\, \cos q \quad , \tag{4.2}$$

where $H_{n,n'}(\underset{\sim}{x})$, $n,n' = 0,1$, is the diabatic electronic potential energy surface. If (N,Q) are the classical action-angle variables of the radiation field, then the theory of the previous chapters gives H_{rad} and H_{int} (in the dipole approximation) as

$$H_{rad} = \hbar\omega N \tag{4.3}$$

$$H_{int} = -\sqrt{\frac{8\pi\hbar\omega}{V}}\, \sqrt{N}\, \sin Q\, \mu(\underset{\sim}{x},n,q) \quad , \tag{4.4}$$

where ω is the frequency of the laser, V the volume of the radiation

cavity, and $\mu(\underset{\sim}{x},n,q)$ is the component of the molecular dipole moment along the polarization vector of the laser. Finally, to express the dipole moment μ as a function of the classical electronic action-angle variables (n,q) we invoke the Heisenberg correspondence relation as discussed by McCurdy and Miller;[37a] this gives

$$\mu(\underset{\sim}{x},n,q) = (1-n)\mu_{00}(\underset{\sim}{x}) + n\mu_{11}(\underset{\sim}{x}) + 2\sqrt{n(1-n)}\,\mu_{01}(\underset{\sim}{x})\,\cos q \quad , \tag{4.5}$$

where $\mu_{n,n'}(\underset{\sim}{x})$, $n,n' = 0,1$ is the matrix of the dipole moment operator in the 2-state electronic basis, as a function of the nuclear coordinates $\underset{\sim}{x}$.

Combining Eqs. (4.1)-(4.5) gives the complete classical Hamiltonian for the nuclear $(\underset{\sim}{p},\underset{\sim}{x})$, electronic (n,q), and photon (N,Q) degrees of freedom as

$$H(\underset{\sim}{p},\underset{\sim}{x},n,q,N,Q) = \frac{\underset{\sim}{p}^2}{2m} + (1-n)H_{00}(\underset{\sim}{x}) + nH_{11}(\underset{\sim}{x}) + 2\sqrt{n(1-n)}\,H_{01}(\underset{\sim}{x})\,\cos q + \hbar\omega N - \sqrt{\frac{8\pi\hbar\omega}{V}}\sqrt{N}\,\sin Q[(1-n)\mu_{00}(\underset{\sim}{x}) + n\mu_{11}(\underset{\sim}{x}) + 2\sqrt{n(1-n)}\mu_{01}(\underset{\sim}{x})\,\cos q]. \tag{4.6}$$

From this Hamiltonian one can numerically integrate Hamilton's equations in the standard way.[13] Initial conditions for the nuclear coordinates and momenta $(\underset{\sim}{x},\underset{\sim}{p})$ are specified in the usual way,[13] and

for the electronic and photon variables, the initial values of n and N are integers, the initial electronic state and the initial number of photons in the radiation field, respectively. If the popular quasiclassical model[13] is employed, then q and Q are chosen initially by Monte Carlo sampling methods. (Section C discusses this in more detail).

For the application in the next section, the Hamiltonian of Eq. (4.6) is simplified following Light et al:[29]

$$H_{01} = \mu_{00}(\underset{\sim}{x}) = \mu_{11}(\underset{\sim}{x}) = 0 \quad . \tag{4.7}$$

Setting $H_{01} = 0$ corresponds to neglecting electronically non-adiabatic effects in the absence of the radiation field, and setting $\mu_{00}(\underset{\sim}{x}) = \mu_{11}(\underset{\sim}{x}) = 0$ corresponds to neglecting the interaction of nuclear motion within a given electronic state with the radiation field (the effect studied in the previous chapter); at the frequency of laser employed here (i.e., visual/UV), this latter interaction is indeed negligible. The quantitites $H_{00}(\underset{\sim}{x})$ and $H_{11}(\underset{\sim}{x})$ are thus the two adiabatic electronic potential energy surfaces $V_0(\underset{\sim}{x})$ and $V_1(\underset{\sim}{x})$, respectively, so that the Hamiltonian of Eq. (4.6) simplifies to

$$H(\underset{\sim}{p},\underset{\sim}{x},n,q,N,Q) = \frac{\underset{\sim}{p}^2}{2m} + (1-n)V_0(\underset{\sim}{x}) + nV_1(x) + \hbar\omega N$$

$$-\sqrt{\frac{8\pi\hbar\omega}{V}}\; 2\sqrt{Nn(1-n)}\; \mu_{01}(\underset{\sim}{x})\; \sin Q \cos q \quad . \tag{4.8}$$

This is the classical Hamiltonian used for the applications in the next section. (The usual Langer-like modification[37]--i.e., in the last term, $\sqrt{n(1-n)} \rightarrow \sqrt{(n+\frac{1}{2})(\frac{3}{2}-n)}$--is also made to Eq. (4.8). N

is so large that replacing N by $N + \frac{1}{2}$ has no significant effect).

C. Classical Trajectory Calculations

Light et al.[29] and later Kulander et al.[31] considered a collinear version of the above reaction, and this is the example we also treat, using the same two potential energy surfaces as these authors used. (The parameters defining the two LEPS potential surfaces are given in Table II of reference 29). The classical Hamiltonian of Eq. (4.8) then defines the collision system, and the calculations reported below were carried out within the standard quasi-classical model.

The methodology of quasi-classical trajectory calculations is well-known.[13] For this example, there are two nuclear degrees of freedom, i.e., $(\underset{\sim}{p},\underset{\sim}{x}) \equiv (P,p,R,r)$, where (R,P) are the coordinate and momentum for relative translation of LiF and H, and (r,p) are the coordinate and momentum for vibration for LiF. $(\tilde{n},\tilde{q})$ denote the vibrational action-angle variables for LiF, and $r(\tilde{n},\tilde{q})$ and $p(\tilde{n},\tilde{q})$ are the algebraic functions which express the cartesian vibrational variables in terms of their action-angle variables.

The initial conditions (at time t_1) for a trajectory are then specified as

$$
\begin{aligned}
n(t_1) &= n_1 \text{ (the electronic quantum number) = 0 or 1} \\
N(t_1) &= N_1 \text{ (the photon quantum number) = integer} \\
q(t_1) &= q_1 \\
Q(t_1) &= Q_1 \\
r(t_1) &= r(\tilde{n}_1,\tilde{q}_1) \\
p(t_1) &= p(\tilde{n}_1,\tilde{q}_1)
\end{aligned}
\qquad (4.9)
$$

where $\tilde{n}_1$ is an integer, the initial vibrational state,

$$R(t_1) = \text{large}$$

$$P(t_1) = \sqrt{2\mu E_{tr}}$$

If $\chi_r(q_1,Q_1,\tilde{q}_1,n_1,n_1,\tilde{n}_1;E_{tr})$ is the characteristic function for reaction--i.e., $\chi_r = 1$ if the trajectory with the indicated initial conditions is reactive, and is 0 otherwise--then the total reaction probability for initial quantum numbers n_1, N_1, $\tilde{n}_1$ and initial translational energy E_{tr} is

$$P_r(n_1,N_1,\tilde{n}_1;E_{tr}) = (2\pi)^{-3}\int_0^{2\pi}dq_1\int_0^{2\pi}dQ_1\int_0^{2\pi}d\tilde{q}_1\ \chi_r(q_1,Q_1,\tilde{q}_1,n_1,N_1,\tilde{n}_1;E_{tr}) \tag{4.10}$$

The integrals over q_1, Q_1, and $\tilde{q}_1$ are performed by Monte Carlo.

The explicit form of Hamilton's equations for the present example are (since Light et al.[29] assume that $\mu_{01}(\underset{\sim}{x}) = \mu_{01}$ is coordinate independent)

$$\begin{aligned}
\dot{r} &= \frac{\partial H}{\partial p} = p/m \\
\dot{R} &= \frac{\partial H}{\partial P} = P/\mu \\
\dot{q} &= \frac{\partial H}{\partial n} = V_1(r,R) - V_0(r,R) - \mu_{01}\sqrt{\frac{8\pi\hbar\omega}{V}}\ \frac{\sqrt{N}(1-2n)}{\sqrt{(n+\frac{1}{2})(\frac{3}{2}-n)}}\ \sin Q\ \cos q \\
\dot{Q} &= \frac{\partial H}{\partial N} = \hbar\omega - \mu_{01}\sqrt{\frac{8\pi\hbar\omega}{V}}\ \frac{\sqrt{(n+\frac{1}{2})(\frac{3}{2}-n)}}{\sqrt{N}}\ \sin Q\ \cos q \\
\dot{p} &= -\frac{\partial H}{\partial r} = -(1-n)\frac{\partial V_0}{\partial r} - n\frac{\partial V_1}{\partial r} \\
\dot{P} &= -\frac{\partial H}{\partial R} = -(1-n)\frac{\partial V_0}{\partial R} - n\frac{\partial V_1}{\partial R}
\end{aligned} \tag{4.11}$$

$$\dot{n} = -\frac{\partial H}{\partial q} = -\mu_{01}\sqrt{\frac{8\pi\hbar\omega}{V}}\; 2\sqrt{N(n+\tfrac{1}{2})(\tfrac{3}{2}-n)}\;\sin Q\,\sin q \quad ,$$

$$\dot{N} = -\frac{\partial H}{\partial Q} = \mu_{01}\sqrt{\frac{8\pi\hbar\omega}{V}}\; 2\sqrt{N(n+\tfrac{1}{2})(\tfrac{3}{2}-n)}\;\cos Q\,\cos q \quad ,$$

which are integrated with our usual variable step-size predictor-corrector algorithm.[21]

Before presenting the results of these trajectory calculations, it is useful to discuss some qualitative aspects of the process. Figure 18 shows a sketch of the energy profiles--the potential energy along a "reaction coordinate"--for the two potential energy surfaces. Referring to this figure, one sees that the ground state potential energy surface has an activation barrier of $\sim$ 0.4 eV, so with no laser present the reaction probability as a function of initial translational energy should have a threshold of $\sim$ 0.4 eV. With a laser of frequency ω, though, the electronic energy gap V_1-V_0 comes into resonance with the laser when classical motion on the (initial) ground state surface reaches the position s_0 indicated in Figure 18, i.e., s_0 is the value for which $V_1-V_0 = \hbar\omega$. For initial translational energies $E_{tr} \geq V_0(s_0)$, therefore, classical motion will reach this position and there will be the possibility of resonant electronic excitation; if this happens, then reaction (to electronically excited $Li^* + HF$) occurs with high probability because motion on the excited potential surface is "downhill all the way" to products.

Qualitatively, therefore, one expects a laser of frequency ω to reduce the threshold of the reaction to approximately $V_0(s_0)$. (Note that for the surfaces in Figure 18 $V_0(s_0)$ decreases with

increasing ω). It is also clear that an initial translational energy $E_{tr} \simeq V_0(s_0)$ is the optimum translational energy for reaction (below the laser-free threshold of $\sim$ 0.4 eV) because in this case the classical motion spends the most time in the resonant region $V_1-V_0 \simeq \hbar\omega$, i.e., for higher translational energies, the classical motion will pass the "resonance region" with finite velocity and thus have a smaller probability of being electronically excited.

The primary qualitative effect of the laser is thus to cause a peak in the reaction probability at the translational energy $E_{tr} \simeq V_0(s_0)$, i.e., where the classical turning point on the ground state potential surface coincides with the resonance region $V_1(s_0)-V_0(s_0) = \hbar\omega$. This is the classical version of a Franck-Condon effect, and one can characterize this behavior semi-quantitatively by calculating the electronic transition probability in the Landau-Zener approximation to the curve-crossing picture in the electronic-field representation.[7] (One considers the two potential curves V_1 and $V_0 + \hbar\omega$). Within this model, the probability of the electronic transition $0 \to 1$ with photon transition $N \to N - 1$ is given by

$$P_{i,N-1\to 0,N} = 1 - e^{-\delta} \tag{4.12}$$

with

$$\delta = \frac{2\pi}{\hbar v} \frac{\mu_{01}^2 \dot{\bar{E}}^2}{|\Delta V_0'|}$$

where

$$\overline{E^2} = \frac{2\pi\hbar\omega N}{V}$$

$$\Delta V_0' = V_1'(s_0) - V_0'(s_0)$$

$$v = \sqrt{\frac{2}{m}\left[E_{tr} - V_0(s_0)\right]}$$

In this approximation the probability of electronic excitation is 0 for $E_{tr} < V_0(s_0)$, jumps to 1 for $E_{tr} = V_0(s_0)$, and then falls for higher E_{tr}.

For still higher translational energies, $E_{tr} \gtrsim 0.4$ eV, the reaction probability will again rise since reaction can then take place on the ground state potential energy surface. Figure 19 shows a sketch of this expected energy dependence of the reaction probability. One can estimate the <u>width</u> of the Franck-Condon peak in the reaction probability near $E_{tr} \simeq V_0(s_0)$ by determining the value of $E_{tr} - V_0(s_0)$ for which $P = \frac{1}{2}$. Using Eq. (4.12), this "half-width" is easily found to be

$$\left[E_{tr} - V_0(s_0)\right]_{P=1/2} = \frac{m}{2}\left[\frac{\mu_{01}^2}{|\Delta V_0'|}\,\frac{\bar{E}^2}{\hbar}\,\frac{2\pi}{\ell n 2}\right]^2 \quad , \tag{4.13}$$

which is seen to be proportional to the square of the laser intensity.

This qualitative discussion above, which is based on the one dimensional picture of the reaction in Figure 18 is modified in several ways when the vibrational degree of freedom is taken into account. Most significantly, the Franck-Condon maximum in the cross section below the laser-free threshold will, in general, be

split into two maxima. This is because the "Franck-Condon region", i.e., the place where the classical motion spends the most time, is now where the vibrational motion, as well as the translational motion, experiences a classical turning point. Vibrational motion has two classical turning points, however, so there will be two points on the ground state potential surface where the translational and vibrational motion simultaneously experience classical turning points (i.e., have zero momenta). The electronic energy gap V_1-V_0 will, in general, be different at these two points, and this leads to two different Franck-Condon maxima. (If there were no translation-vibration coupling in the potential energy surfaces and if the vibrational potential functions for the two electronic states were the same, then V_1-V_0 would be the same at the two simultaneous translation-vibration turning points and the two Franck-Condon maxima would be coincident). This will be seen more explicitly later in this discussion.

Figure 20 shows the total reaction probability as a function of initial translational energy for the quasi-classical trajectory model as described above. LiF is always in its ground vibrational state initially. The dotted curve is the laser-free result, showing the expected threshold at $\sim$ 0.4 eV. The solid curve is obtained for a laser with frequency $\hbar\omega$ = 6.2 eV and a power such that $\mu_{01}E_0$ = 0.01 eV ($E_0 = \sqrt{8\pi\hbar\omega N_1/V}$), and the dashed curve is the result for a laser of the same frequency but lower power, $\mu_{01}E_0$ = 0.008 eV.

Both laser-induced curves in Figure 20 show the two Franck-Condon maxima as discussed at the end of the previous section, and the

height and width of the peaks increase with increasing laser power. At the still lower power corresponding to $\mu_{01}E_0 = 0.001$ eV, the peaks have disappeared.

The Franck-Condon peaks in Figure 20 show the asymmetric "line shape" suggested by the Landau-Zener model discussed above with increasing translational energy, the reaction probability rises almost vertically to a maximum and then falls more gradually. Quantum mechanical effects may, of course, modify this structure in some of its details, but the gross features are expected to persist in a quantum description.

Figure 21 illustrates the effect of varying the laser frequency. (The laser-free reaction probability is also shown again here). For a power corresponding to $\mu_{01}E_0 = 0.01$ eV, the solid curve is for a frequency $\hbar\omega = 6.2$ eV (the same curve as shown in Figure 20), and the dashed curve is for a frequency $\hbar\omega = 6.4$ eV. The higher frequency is thus seen to lead to a lower threshold for reaction, as is understood from the discussion above. A surprise though, is that the higher frequency (dashed curve in Figure 21) has only one peak, not two, in the region below the laser-free threshold.

To understand this latter feature and to confirm that our interpretation of these "Franck-Condon maxima" is actually correct, we computed laser-free classical trajectories on the ground state potential energy surface to determine the Franck-Condon transition points. For a given translational energy E_{tr} (and with LiF initially in its ground vibrational state) the initial vibrational angle variable was varied over its range $(0,2\pi)$ to determine the two points, (r_1,R_1) and (r_2,R_2), at which translation and vibration

have simultaneous classical turning points. The electronic energy gaps, V_1-V_0, at these two points define <u>two</u> frequencies, via $\hbar\omega = V_1-V_0$, for which E_{tr} is a Franck-Condon maximum.

Figure 22 shows, as a function of translational energy E_{tr}, these two frequencies $\hbar\omega = V_1(R_k,r_k) - V_0(R_k,r_k)$, where (R_k,r_k), $k = 1,2$ are the two simultaneous turning points for energy E_{tr}. A horizontal line at a given frequency then gives the two translational energies at which Franck-Condon maxima should appear for that laser frequency.

For frequency $\hbar\omega = 6.2$ eV, Figure 22 thus indicates that Franck-Condon maxima should appear at $E_{tr} \simeq 0.15$ eV and 0.19 eV, and from the Landau-Zener discussion it is clear that these are actually the energies at which the reaction probability has its sharp vertical rise at these energies.

For the higher frequency, $\hbar\omega = 6.4$ eV, Figure 22 indicates the two Franck-Condon energies to be $E_{tr} \simeq 0.116$ eV and 0.15 eV. The reaction probability for this frequency (dashed curve in Figure 21) does indeed show a sharp rise at $E_{tr} \simeq 0.116$ eV and also a broadened structure at $E_{tr} \simeq 0.15$ eV, but it is clear that this is a case for which the two Franck-Condon maxima have merged into a single broadened peak.

It seems clear, therefore, that this Franck-Condon picture of the structure in the reaction probability is physically correct. Note however that quantum mechanically the lowest vibrational state is not peaked at the classical turning points so only one peak is expected. Recent quantum mechanical studies of this system have found a peak at the "outer" (that is "small r" vibrational turning

point). These results are in qualitative agreement with the classical results.[31]

In the three-dimensional calculations the equations of motion become slightly more complicated. As in the collinear case $\mu_{01}(\underset{\sim}{x})$ is taken as a constant. However

$$\mu_{01}(\underset{\sim}{x}) = \vec{\mu}_{01} \cdot \hat{\epsilon} = \mu_{01}(\hat{\mu} \cdot \hat{\epsilon}) \tag{4.14}$$

where $\vec{\mu}_{01}$ is a vector of constant magnitude μ_{01} in a direction $\hat{\mu}$ which is perpendicular to the plane of the three atom system. Therefore $\frac{\partial \mu_{01}(\underset{\sim}{x})}{\partial \underset{\sim}{x}}$, where $\underset{\sim}{x}$ is the vector of coordinates of the particles, is no longer zero as in the collinear case but a function of the relative positions of the atoms.

Besides this additional complication the calculation is carried out using standard quasi-classical trajectory methods[13] (which have been described elsewhere) with the inclusion of the four equations of motion describing the laser field and electronic degree of freedom.

It was found that the cross-sections for three-dimensional LiF + H on the ground state surface without the field were extremely small. The cross-section at one laser intensity and several laser frequencies is compared to that without the field in Figure 23. The threshold for reaction was lowered in all cases. There was no significant variation found with the polarization of the laser field. At most frequencies there were no low translational energy peaks and those that occurred were significantly reduced. This is due in part to the three-dimensional nature of the problem since the simple

vibrational/translational turning point structure is washed out by the rotation of the system. Also, the motion on the ground state is primarily repulsive for many of the approach parameters so the system cannot enter into a favorable region for excitation to the upper potential energy surface.

D. Laser Inhibition of Chemical Reactions

The model used in this calculation is very similar to that described by Light, et al.[29] The ground state surface was taken to be the Karplus-Porter potential surface for $H + H_2$.[14] The excited state was taken to be a LEPS surface for $H + H_2$ shifted upward by 0.5 eV but with the Sato parameter δ as 0.20. The effect of this change is to lower the barrier to reaction and shift the reaction path slightly. As described in the previous section it is possible to predict for a given laser frequency the resonant translational energies, that is the translational energies where transitions to the excited potential energy come into resonance causing a peak in the reactive probability. Figure 24 shows the difference between the two potential energy surfaces at the vibrational/translational turning points for the system as a function of translational energy. To obtain the translational energies where the Franck-Condon like factors are favorable for transition to the upper surface, a horizontal line is drawn across the graph at the laser frequency.

A quasi-classical calculation was carried out for this system as described in the previous section. In Figure 25 the probability of transition to the excited potential energy surface as a function

of translational energy is plotted for one laser field strength and a series of laser frequencies. Peaks occur at the predicted translational energies.

So far only the effect of the laser on the reactive probability on the lower surface has been considered. It is also possible to study the effect of the laser on the reaction probability on the excited surface. At the laser frequencies and field strengths studied for LiF + H the effect was small, due to the large differences in the potential energy surfaces. However in this model the two potential energy surfaces are very similar so the region of favorable interaction overlaps considerably. In Figure 26 the reaction probability in the presence of the field at several laser frequencies is compared to that of the field-free case. There is significant inhibition of reaction on the upper state potential energy surface. In Figure 27 this effect is illustrated as a function of field strengths. For even quite low field strengths ($\mu \cdot E = 0.001$ eV) the effect is still pronounced. It is important to note that the largest probability for transition to the upper state potential energy surface from the lower surface occurs where a large inhibition of the reaction probability on the upper surface occurs. These two effects tend to cancel, resulting in the reaction probability on the lower surface shown in Figure 28. Quantum mechanically a similar effect occurs, however a residual peak is still seen at the positions marked in Figure 24.[31] It is interesting to note that these again occur at the "small r" (outer) turning point.

E. Effect of Isotopic Substitution

In this section results on the effect of isotopic substitution on the enhancement of chemical reactions via a collision induced absorption is discussed. The system studied is the same as that used in Section II but with the hydrogen replaced with deuterium. All other parameters remained the same. In Figure 29 the results for LiF + D are compared to those of LiF + H for one laser frequency and field strength. As can be seen, the peak is shifted and narrowed. This suggests the interesting possibility that isotopic-specific enhancement may occur during a chemical reaction.

F. Conclusion

The purpose of this paper was to illustrate the use of a completely classical model to study the laser enhancement of chemical reactions via a collision induced absorption. Because calculations can be carried out within the standard quasi-classical framework, it was relatively easy to apply this model to a wide range of collinear and three-dimensional systems. When comparison was made to the available quantum mechanical results, they were found to be in qualitative agreement though the quantitative agreement was much worse.[29,31] As will be illustrated by the next chapter, the classical model while correctly predicting positions of peaks, has the heights of the peaks always too large. Therefore this method does as well (or as poorly) as do other quasiclassical studies of more conventional processes (such as vibrational or rotational excitation during a molecular collision).

However the quantum mechanical calculation can only be carried out on simple collinear systems. It is not possible (at present) to carry out quantum mechanical three-dimensional calculations on these systems, whereas the classical calculation is relatively simple to perform.

The Franck-Condon structure in the cross section is certainly the most interesting feature revealed by the present calculations. The fact that a laser of frequency ω will significantly enhance the reaction probability at a particular collision energy E_{tr} (more precisely, in a narrow range of collision energies) is an important point to be aware of: knowing how this Franck-Condon energy varies with ω provides fairly direct information about the potential energy surfaces that are involved in the process, and in a molecular beam experiment, for example, the laser-induced effect will be largest when the collision energy is "tuned" to this Franck-Condon region. It is in predicting this Franck-Condon structure that the method is the most accurate. A simple calculation, even in regions where the classical probability is very small, can predict the Franck-Condon structure in the quantum mechanical reaction probabilities.

The other interesting feature pointed out in this chapter include isotopic selectivity in these Franck-Condon peaks a result reflected in the quantum mechanical studies,[31] as well as a strong laser inhibition of a chemical reaction. These effects seem to be quite general and are expected to be seen in other systems. The laser inhibition or chemical reaction is of particular interest as the effect is still noticeable for small field strengths (of the order of megawatts) and hence could be possibly seen experimentally in some systems.

V. RESONANCE EFFECTS IN ELECTRONIC-VIBRATIONAL ENERGY TRANSFER

A. Introduction

This final chapter illustrates another example of a completely classical model for all degrees of freedom of a collinear system. A series of papers[37] over the last few years has developed and applied a classical model for treating electronically non-adiabatic processes in molecular collisions. The novel feature of this model is that electronic, as well as heavy particle (i.e., translation, rotation, and vibration), degrees of freedom are described by classical mechanics, and its attractiveness from a practical point of view is that calculations can be carried out within the framework of standard Monte Carlo classical trajectory methodology.[13]

One of the motivations for developing this completely classical model was the realization[38] that "mixed" dynamical models--i.e., those which characterize some degrees of freedom by classical mechanics and others by quantum mechanics--fail to describe some features of the dynamics correctly. The very popular and often successful surface-hopping model,[39] for example, which treats heavy particle motion classically but electronic degrees of freedom quantum mechanically (as states, i.e., distinct potential energy surfaces) is unable to describe resonance effects between electronic and heavy particle degrees of freedom. Such resonance effects are important in the quenching of excited fluorine atoms ($^2P_{1/2}$) by collision with H_2[40] because the 404 cm^{-1} excitation energy of fluorine is roughly equal (within $\sim$ 10%) to the energy of the $0 \rightarrow 2$ rotational excitation of H_2. Similarly, $Br^*(^2P_{1/2})$ is thought[41] to be quenched efficiently by H_2 because

the vibrational quantum of H_2 approximately matches the 3685 cm^{-1} excitation energy of bromine. Since the classical model[37] treats all degrees of freedom on the same dynamical footing, i.e., by classical mechanics, it has been reasoned that it should be able to describe these aspects of resonance energy transfer at least qualitatively correctly. To see how quantitative the model is, however, requires numerical applications, and such is the purpose of this chapter.

Earlier calculations[37d] have shown that the classical model does indeed provide a reasonably good description of the resonance effect between electronic and rotational degrees of freedom in $F-H_2$ collisions,

$$F^*(^2P_{1/2}) + H_2(j=0) \rightarrow F(^2P_{3/2}) + H_2(j=2) \quad ; \quad (5.1)$$

The cross section for this process is much larger at low collision energies than for quenching by a comparable rare gas atom that does not have rotational degrees of freedom. The present paper considers a simple model of electronic-vibrational energy transfer that would pertain, for example, to the quenching of Br^* by H_2,

$$Br^*(^2P_{1/2}) + H_2(v=0) \rightarrow Br(^2P_{3/2}) + H_2(v=1) \quad . \quad (5.2)$$

The particular example we consider is the collinear version of such a system for which Lee, Lam, DeVries, and George[42] have recently carried out quantum mechanical coupled channel calculations. Lee et al.'s calculations provide the exact results for this model problem, which can thus serve as a benchmark to see how well the classical model is able to describe such non-adiabatic processes.

Section B defines the system treated by Lee et al. and briefly

summarizes the classical model as it applies to this example. The results are discussed in Section C.

B. The Classical Model

Lee et al.[42] consider a collinear atom-diatom collision system, A + BC, with two potential energy surfaces, i.e., two electronic states, corresponding to ground and excited states of the atom A. The 2 x 2 diabatic interaction potential surface is

$$\begin{pmatrix} V_{00}(R,r) & V_{01}(R,r) \\ V_{10}(R,r) & V_{11}(R,r) \end{pmatrix} = \begin{pmatrix} \frac{\lambda}{3} & \frac{\sqrt{2}\,\lambda}{3} \\ \frac{\sqrt{2}\,\lambda}{3} & \frac{2\lambda}{3} \end{pmatrix}$$

$$+ e^{-\alpha(R - \frac{1}{2} r - p_0)} \begin{pmatrix} A_0 & 0 \\ 0 & A_1 \end{pmatrix} , \qquad (5.3)$$

where r is the vibrational coordinate of BC and R the translational coordinate, the distance of A to the center of mass of BC. It is useful to make a unitary transformation of this potential matrix to diagonalize the first term, the atomic part of the interaction that survives as $R \to \infty$. The appropriate unitary transformation matrix is

$$\underset{\approx}{U} = \begin{pmatrix} \sqrt{\frac{2}{3}} & \sqrt{\frac{1}{3}} \\ -\sqrt{\frac{1}{3}} & \sqrt{\frac{2}{3}} \end{pmatrix} , \qquad (5.4)$$

and for the transformed potential matrix $\underset{\approx}{\bar{V}}$,

$$\bar{\bar{V}} \equiv \bar{\bar{U}}^{\dagger} \cdot \bar{\bar{V}} \cdot \bar{\bar{U}} \quad , \tag{5.5}$$

one obtains

$$\begin{pmatrix} \bar{V}_{00} & \bar{V}_{01} \\ \bar{V}_{10} & \bar{V}_{11} \end{pmatrix} = \begin{pmatrix} 0 & 0 \\ 0 & \lambda \end{pmatrix} + e^{-\alpha(R-\frac{1}{2}r-\rho_0)} \begin{pmatrix} \bar{A}_{00} & \bar{A}_{01} \\ \bar{A}_{10} & \bar{A}_{11} \end{pmatrix} , \tag{5.6}$$

where

$$\bar{A}_{00} = \frac{2}{3} A_0 + \frac{1}{3} A_1 \tag{5.7a}$$

$$\bar{A}_{11} = \frac{1}{3} A_0 + \frac{2}{3} A_1 \tag{5.7b}$$

$$\bar{A}_{01} = \bar{A}_{10} = \frac{\sqrt{2}}{3} (A_1 - A_0) \quad . \tag{5.7c}$$

The classical model[37] for the electronic degrees of freedom replaces the diabatic potential matrix $\bar{V}_{N,N'}(R,r)$, N,N' = 0,1 of Eq. (5.3) by a classical electronic Hamiltonian $\bar{V}(R,r,N,Q)$ which is defined in terms of the matrix elements by

$$\bar{V}(R,r,N,Q) = N\bar{V}_{11}(R,r) + (1-N)\bar{V}_{00}(R,r)$$

$$+ 2\, \bar{V}_{01}(R,r) \sqrt{(N+\tfrac{1}{2})(\tfrac{3}{2}-N)} \quad \cos Q \quad . \tag{5.8}$$

(N,Q) are the classical action-angle variables[11] for the electronic degrees of freedom; i.e., N is the classical electronic quantum number. With Eq. (5.6) one notes that as $R \to \infty$ Eq. (5.8) becomes

$$\bar{V}(R\to\infty,r,N,Q) = N\lambda \quad ; \tag{5.9}$$

thus N is a conserved quantity in the asymptotic region, with N=0 corresponding to the ground electronic state of atom A (with energy

0) and N=1 to the excited state A^* (with energy λ).

To obtain the classical Hamiltonian for the complete system one adds to $\bar{V}(R,r,N,Q)$ the potential energy for free vibrational motion of BC and the kinetic energy for vibration and translation, and with Eqs. (5.6) and (5.8) this gives

$$H(P,R,p,r,N,Q) = \frac{P^2}{2\mu} + \frac{p^2}{2m} + \frac{1}{2}m\omega^2(r-r_0)^2$$

$$+ N\lambda + e^{-\alpha(R-\frac{1}{2}r-\rho_0)}[(1-N)\bar{A}_{00} + N\bar{A}_{11}$$

$$+ 2\bar{A}_{01}\sqrt{(N+\tfrac{1}{2})(\tfrac{3}{2}-N)}\cos Q] \quad . \qquad (5.10)$$

where m and μ are the reduced masses for BC vibration and A-BC translation, respectively. To obtain the final form of the classical Hamiltonian one replaces the vibrational coordinate and momentum (r,p) by their action-angle variables[11] (n,q),

$$r-r_0 = \sqrt{\frac{2n+1}{m\omega}}\cos q \qquad (5.11a)$$

$$p = -\sqrt{(2n+1)m\omega}\sin q \quad , \qquad (5.11b)$$

giving

$$H(P,R,n,q,N,Q) = \frac{P^2}{2\mu} + (n+\tfrac{1}{2})\omega + N\lambda$$

$$+ \exp[-\alpha[R-R_0-\tfrac{1}{2}\sqrt{\frac{2n+1}{m\omega}}\cos q]][(1-N)\bar{A}_{00} + N\bar{A}_{11}$$

$$+ 2\bar{A}_{01}\sqrt{(N+\tfrac{1}{2})(\tfrac{3}{2}-N)}\cos Q] \quad . \qquad (5.12)$$

The results presented in the next section corresponds to implementation of the classical model within the framework of the standard quasiclassical histogram approach.[13,21] Thus to compute the probability for the following vibration-to-electronic transition,

$$A + BC(n=1) \rightarrow A^* + BC(n=0) \quad , \tag{5.13}$$

one integrates Hamiltonian's equations (generated from the Hamiltonian of Eq. (5.12) with initial conditions

$$\begin{aligned} n(t_1) &= 1 \equiv n_1 \\ N(t_1) &= 0 \equiv N_1 \\ q(t_1) &= 2\pi\xi_1 \\ Q(t_1) &= 2\pi\xi_2 \\ R(t_1) &= \text{large} \\ P(t_1) &= -\sqrt{2\ [E_{tr}-(n_1+\tfrac{1}{2})\ -N_1\lambda]} \end{aligned} \quad . \tag{5.14}$$

where ξ_1 and ξ_2 are random numbers in (0,1) and E_{tr} is the initial tran lational energy. The final values of n and N that correspond to Eq. (5.13) are n=0, N=1, and the quasiclassical approximation to the probability of this transition is the fraction of trajectories with the above initial conditions that have their actual final values of n and N within a "box" of unit width about these values n=0, N=1.

The parameters in the classical Hamiltonian, Eq. (5.12), which correspond to Lee et al.'s[42] calculations are

$$\omega = 0.02 \qquad \alpha = 3$$

$$R_0 = 4.7 \qquad \bar{A}_{00} = \frac{11}{3} \times 10^{-5}$$

$$m = 1000 \qquad \bar{A}_{11} = \frac{13}{3} \times 10^{-5}$$

$$\mu = 3896.1 \qquad \bar{A}_{01} = \frac{2\sqrt{2}}{3} \times 10^{-5} \quad (5.15)$$

These values, in atomic units, correspond roughly to the Br-H_2 system. The parameter λ, the $A \rightarrow A^*$ excitation energy, is varied in these model calculations to assess the significance of resonance in the electronic-vibrational energy transfer. Exact resonance, for example, corresponds to $\lambda = \omega = 0.02$, so for very low translational energies, where resonance considerations are most important, one would expect the transition probability for Eq. (5.13) to be largest for $\lambda \simeq 0.02$. By varying λ one can see how prominent the resonance effect is and how well the classical model is able to describe it.

C. Results and Discussion

Figures 30-32 show the transition probability for Eq. (5.12) as a function of the atomic energy gap λ for translational energies of 0.01 eV, 0.035 eV, and 0.055 eV, respectively. The solid curves are the exact quantum mechanical results computed by Lee et al.,[42] and the broken curves the present results of the classical model. As expected, the resonance structures is sharpest at the lowest translational energy; i.e., in Figure 30 the transition probability peaks sharply at $\lambda \cong 0.02$. At higher translational energy the resonance structure broadens and shifts.

The significant point to note is that this classical model does describe the resonance features in this process reasonably well. The position and width of the resonance peak are described well over the entire energy range considered. Used in this primitive histogram mode, however, the classical results do have shortcomings:

the peak heights are too large (by a factor of two in the worst case, Figure 1) and the classical results do not describe the wings of the resonance line shape well. This latter failing is typical of all quasiclassical histogram treatments, namely the inability to describe weak (classically forbidden) processes.[21]

The encouraging note is that the quasiclassical results for this electronically inelastic process are no worse than typical quasiclassical results for rotationally and vibrationally inelastic processes.[43] Thus the classical model for electronic degrees of freedom seems to do about as well (or as poorly, depending on one's point of view) in describing electronically inelastic processes as classical mechanics does for inelastic processes involving only heavy particle degrees of freedom. To the extent that this level of accuracy is sufficient one thus has a consistent dynamical model for treating both electronically non-adiabatic as well as adiabatic collision processes.

Table I. Dependence of Threshold Lowering on Laser Frequency.

Laser Frequency (cm^{-1})	ΔE_{th} (eV)[a]					
	$H + H_2$	$F + H_2$	$H + HF$	$C\ell + H_2$	$H + HC\ell$	$C\ell + H_2$ 3-dimensional
47	--	--	--	0.13	--	--
94	0.05	> 0.05	0.03	0.12	0.04	0.07
219	0.06	--	--	--	--	--
472	--	0.01	0.03	0.05	0.02	0.03
519	0.09	--	--	--	--	--
768	0.08	--	--	--	--	--
944	0.07	0	0.02	0.01	0.01	0.01
2195	0.01	--	--	--	--	--

[a] Amount by which the threshold of the reaction is lowered by a laser field of a power corresponding to $\hbar\omega_R = 0.1$ eV.

Table II. LEPS Parameters for Potential Energy Surfaces.

	H-H-F		H-H-Cℓ	
	HF	HH	HCℓ	HH
D_e(kcal/mole)	140.5	109.5	106.41	109.43
$\beta(\text{Å}^{-1})$	2.22	1.94	1.87	1.94
$r_0(\text{Å})$	0.917	0.742	1.27	0.742
Δ	0.150	0.080	0.187	0.167

Table III. Parameters for the HX Dipole Moment Function.

	C_n	
n	HF	HCℓ
0	2.35	- 236.95
1	- 3.40	1151.69
2	- 40.16	-2011.50
3	112.15	1631.43
4	- 87.97	- 635.97
5	30.31	101.24

$\alpha = 2.5 \text{ bohr}^{-1}$.

Table IV. LEPS parameters for $H + H_2$ potential energy surface.

D_e(kcal/mole)	109.5
$\beta(\mathring{A}^{-1})$	1.942
$r_0(\mathring{A})$	0.7417
Δ	0.1413

FIGURE CAPTIONS

1. Sketch of a one-dimensional potential energy barrier. x_1 is the initial position and E_1 the initial energy.
2. Reaction probability as a function of initial translational energy [as given by Eq. (2.13] for the one-dimensional model problem.
3. (a) Sketch of the time dependence of the dipole moment of the H-H-H system along a reactive trajectory $H + H_2 \rightarrow H_2 + H$.
   (b) Sketch of the absorption spectrum corresponding to the time-dependent dipole in (a).
4. Reaction probability for the collinear $H + H_2 \rightarrow H_2 + H$ reaction as a function of initial translational energy, without the laser field (——) and with it (---); $\hbar\omega = 944\ cm^{-1}$ and $\hbar\omega_R = 0.1$ eV.
5. Same as Figure 4 except for the reaction $F + H_2(v=0) \rightarrow HF + H$; $\hbar\omega = 94\ cm^{-1}$ and $\hbar\omega_R = 0.1$ eV.
6. Same as Figure 4 except for the reaction $H + HF(v=2) \rightarrow H_2 + F$; $\hbar\omega = 94\ cm^{-1}$ and $\hbar\omega_R = 0.1$ eV.
7. Same as Figure 4 except for the reaction $Cl + H_2(v=0) \rightarrow HCl + H$; $\hbar\omega = 94\ cm^{-1}$, and $\hbar\omega_R = 0.01$ eV and 0.1 eV as labeled.
8. Same as Figure 4 except for the reaction $H + HCl(v=0) \rightarrow H_2 + Cl$; $\hbar\omega = 94\ cm^{-1}$ (•••), $472\ cm^{-1}$ (---), and $\hbar\omega_R = 0.1$ eV.
9. Reactive cross section for the three-dimensional reaction $Cl + H_2 \rightarrow HCl + H$ as a function of initial translational energy, without the laser (——) and with it (---); $\parallel$ and $\lfloor$ indicate the cases of parallel and perpendicular polarization vector of the laser to the initial relative velocity vector, respectively. $\hbar\omega = 94\ cm^{-1}$, $\hbar\omega_R = 0.1$ eV.

10. Correlation function $C(\Delta t)$ for the one-dimensional barrier in the reactive (R, $E_1 > 0$) and non-reactive (NR, $E_1 < 0$) cases.
11. Absorption spectrum corresponding to the correlation function in Figure 10.
12. Correlation function for <u>non-reactive</u> trajectories of the collinear $H + H_2$ collision.
13. Absorption spectrum corresponding to the correlation function in Figure 12.
14. Correlation function for <u>reactive</u> trajectories of the collinear $H + H_2$ collision.
15. Absorption spectrum corresponding to the correlation function in Figure 14.
16. Correlation function for the modified $H + H_2$ potential surface.
17. Absorption spectrum corresponding to the correlation function in Figure 16.
18. Sketch of the potential energy along the reaction coordinate s for the two electronic potential energy surfaces for the system $H + LiF \rightarrow HF + Li$. E_{tr} denotes the initial translational energy and ω the frequency of the laser.
19. Sketch of the qualitative dependence of the total reaction probability on initial translational energy E_{tr}.
20. Total reaction probability for $H + LiF \rightarrow HF + Li$ as a function of the initial translational energy E_{tr}, from a quasi-classical trajectory calculation. LiF is initially in its ground vibrational state. The dotted curve is the laser-free result. The other two curves are for a laser frequency $\hbar\omega = 6.2$ eV, the laser power being such that $\mu_{01}E_0 = 0.01$ eV (solid curve) and 0.008 eV

(dashed curve).

21. Total reaction probability as in Figure 20. The dotted curve is the laser-free result as in Figure 20. The other two curves are for a laser power such that $\mu_{01}E_0 = 0.01$ eV and a frequency $\hbar\omega = 6.2$ eV (solid curve) and $\hbar\omega = 6.4$ (dahsed curve).

22. Shown are the two Franck-Condon frequencies $\hbar\omega \equiv V_1(R_k,r_k) - V_0(R_k,r_k)$, where (R_k,r_k), $k = 1,2$, are the two simultaneous translation-vibration turning points on the ground state potential surface, as a function of the initial translational energy E_{tr}. The intersection of the dashed line at frequency $\hbar\omega = 6.4$ eV with the two curves gives the two translation energies at which Franck-Condon maxima should appear for that laser frequency, and similarly for frequency $\hbar\omega = 6.2$ eV.

23. Total cross-section (a_0^2) for three-dimensional H + LiF → HF + Li as a function of the initial translational energy E_{tr}, from a quasi-classical trajectory calculations. LiF is initially in its ground vibrational-rotational state. The dotted curve is the laser-free result. The other two curves are for a laser power such that $\mu_{01}E_0 = 0.01$ eV and a frequency $\hbar\omega = 6.5$ eV (solid curve) and 6.2 eV (dashed curve).

24. Shown are the Franck-Condon frequencies $\Delta V \equiv V_1(R_k,r_k) - V_0(R_k,r_k)$ where (R_k,r_k), $k = 1,2$ are the two simultaneous translation-vibration turning points on the ground state potential surface, as a function of the initial translational energy, E_{tr}, for the model system with H + H_2 parameters. The position of peaks in the quantum mechanical probability for $\mu_{01}E_0 = 0.01$ are marked by crosses.

25. The probability for transition to the upper state potential surface for the model $H + H_2$ system as a function of the initial translational energy E_{tr}, from a quasi-classical trajectory calculation. H_2 is initially in its ground vibrational state. The curves are for a laser power such that $\mu_{01}E_0$ = 0.01 eV and a frequency $\hbar\omega$ = 0.017 a_0 (solid curve), 0.0165 a_0 (dashed curve) and 0.016 a_0 (dash-dot curve).

26. Total reaction probability on the upper state surface for the model $H + H_2$ system as a function of initial translational energy, E_{tr}, from a quasi-classical calculation. H_2 is initially in its ground vibrational state. The dotted curve is the laser-free result. The curves are for a laser power such that $\mu_{01}E_0$ = 0.01 eV and frequency $\hbar\omega$ = 0.017 a_0 (solid curve), 0.0165 a_0 (dashed curve) and 0.016 a_0 (dot-dash curve).

27. Total reaction probability as in Figure 26. The dotted curve is the laser-free result as in Figure 26. The laser frequency is $\hbar\omega$ = 0.017 a_0 and the laser field strength is such that $\mu_{01}E_0$ = 0.01 eV (solid curve), 0.005 eV (dashed curve) and 0.001 eV (dash-dot curve).

28. Total reaction probability on the state surface for the model $H + H_2$ system as a function of initial translational energy, E_{tr}, from a quasi-classical calculation. H_2 is initially in its ground vibrational state. The dotted curve is the laser-free result. The curves are for a laser power such that $\mu_{01}E_0$ = 0.01 eV and frequency $\hbar\omega$ = 0.017 a_0 (solid curve), 0.0165 a_0 (dashed curve) and 0.016 a_0 (dash-dot curve).

29. Total reaction probability for collinear LiF + H → HF + Li

(solid curve) and collinear LiF + D → DF + Li (dashed curve) as a function of initial translational energy, E_{tr}, from a quasi-classical calculation. LiF is initially in its ground vibrational state. The curves are for a laser power such that $\mu_{01}E_0$ = 0.01 eV and a laser frequency $\hbar\omega$ = 6.2 eV.

30. Transition probability for Eq. (2.11) as a function of the atomic excitation energy λ, for an initial translational energy E_{tr} = 0.01 eV. The solid curve is the exact quantum result of Lee et al. (reference 42) and the broken curve the results of the present classical model; the error bar is the usual Monte Carlo error estimate.

31. Same as Figure 30 except E_{tr} = 0.035 eV.

32. Same as Figure 30 except E_{tr} = 0.055 eV.

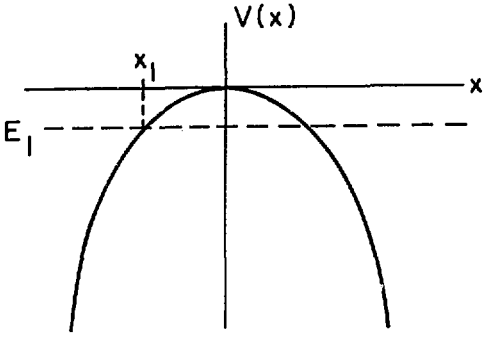

XBL 7812-14071

Figure 1

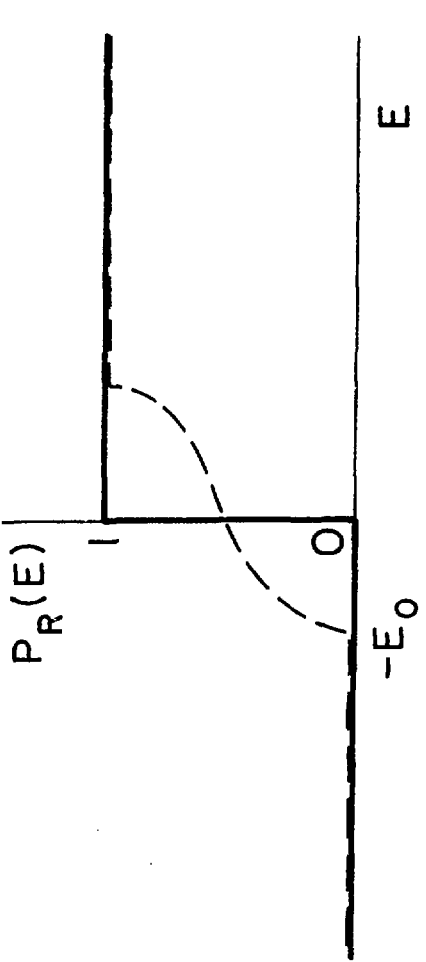

XBL 783-7788

Figure 2

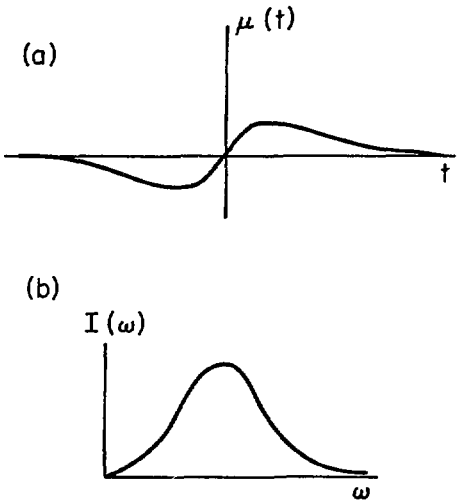

XBL 7812-14072

Figure 3

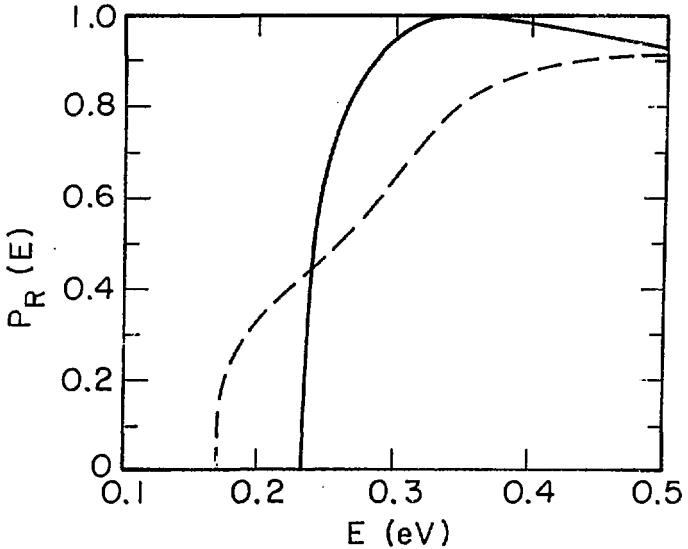

XBL 783-7789

Figure 4

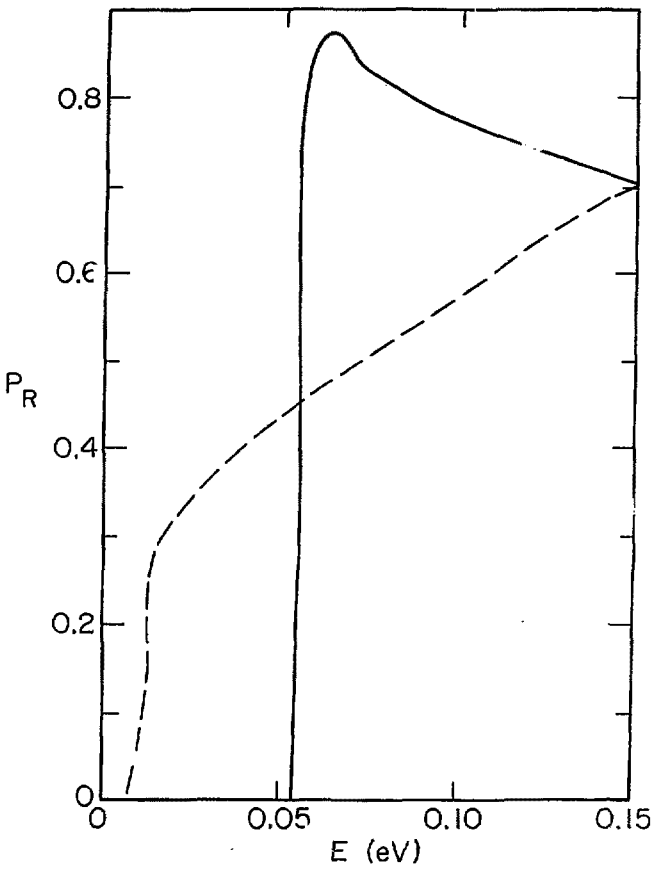

Figure 5

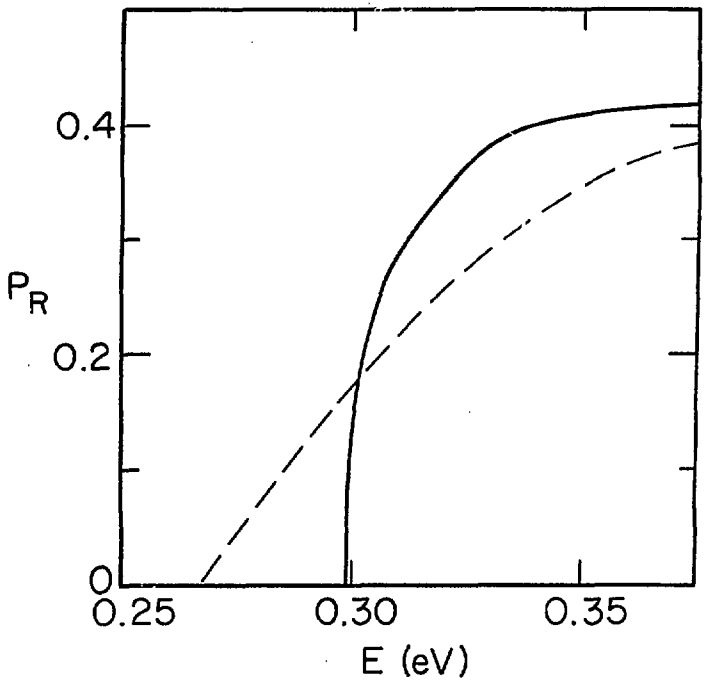

XBL 7812-14073

Figure 6

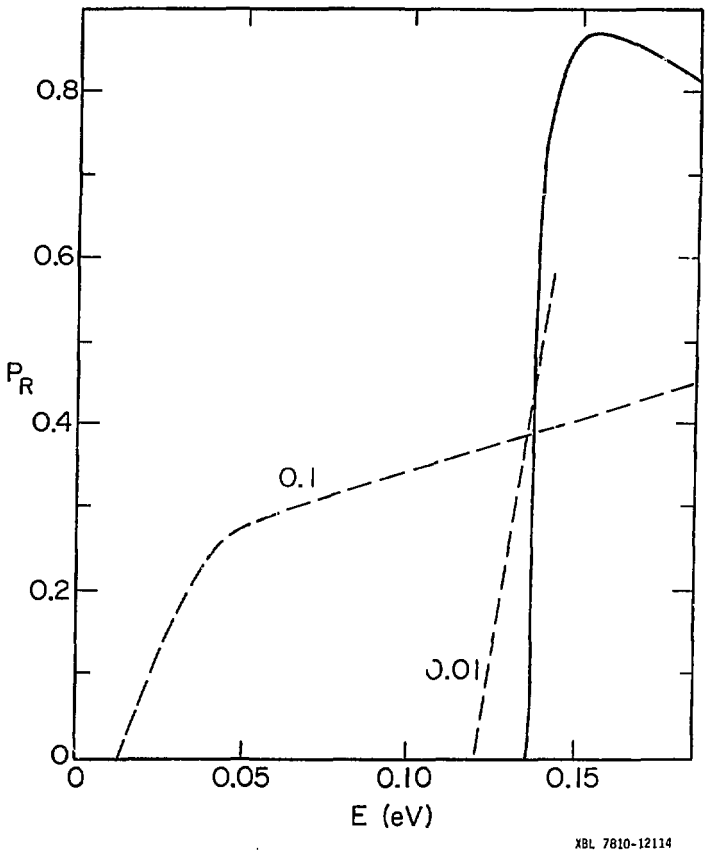

Figure 7

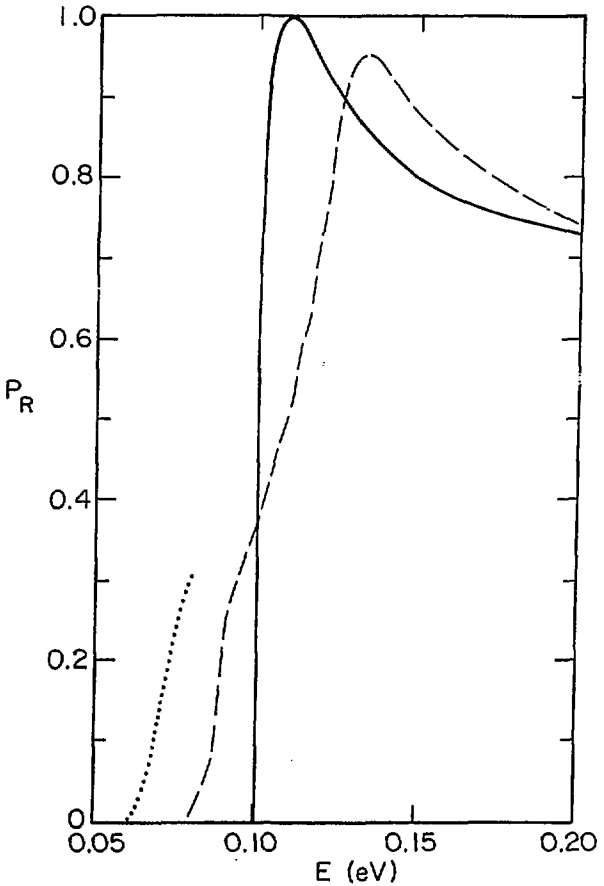

XBL 7812-14075

Figure 8

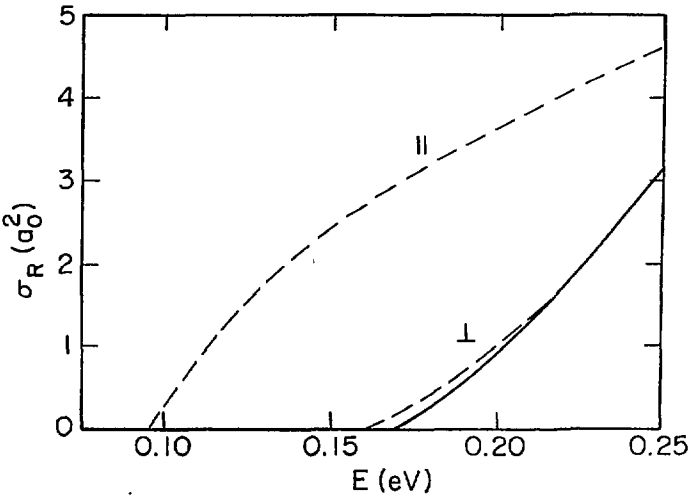

Figure 9

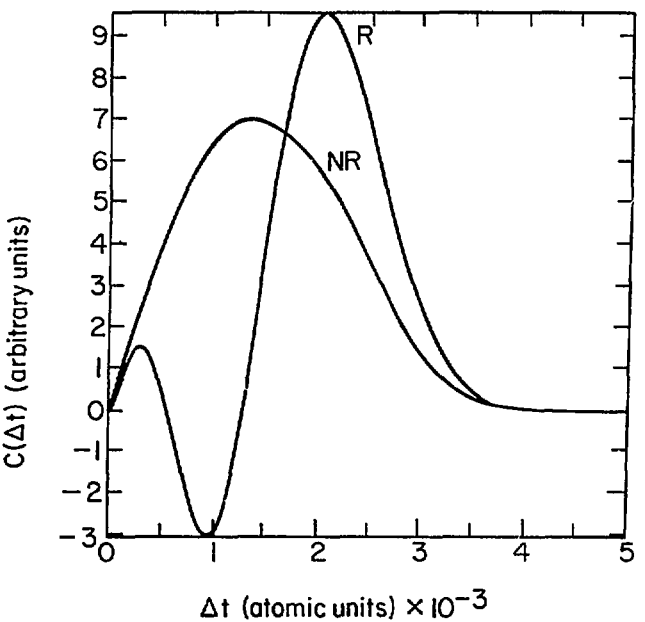

XBL 7911-12750

Figure 10

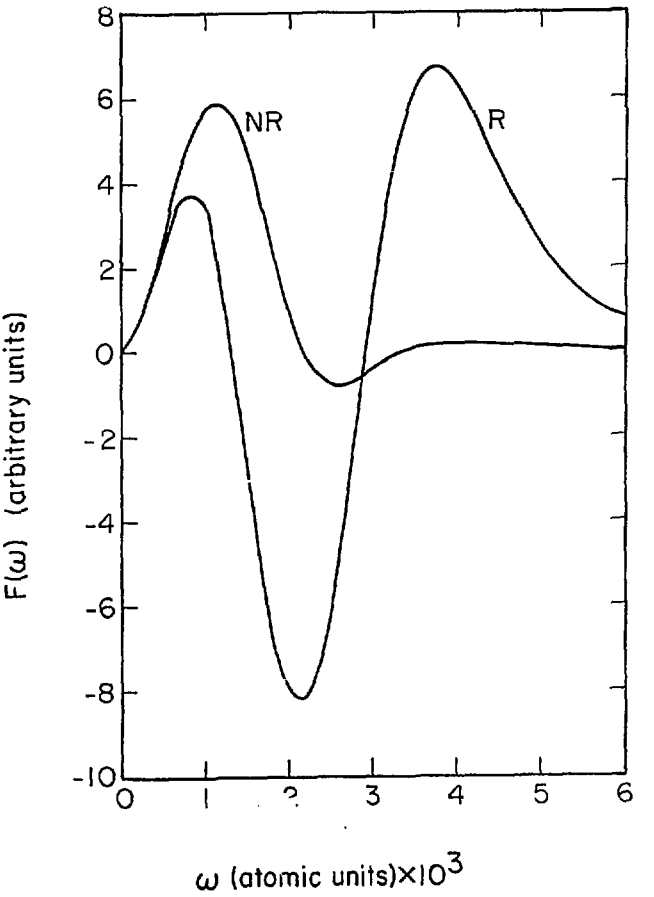

XBL 7911-12746

Figure 11

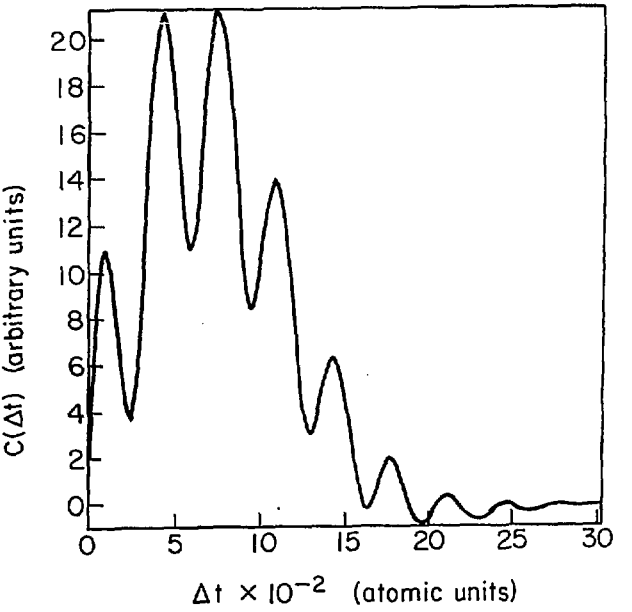

XBL 7911-12749

Figure 12

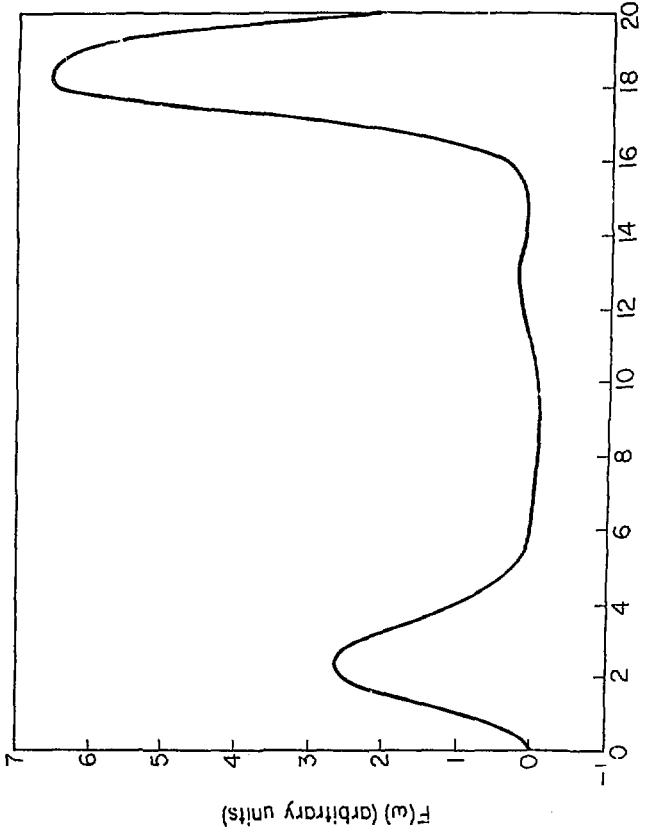

XBL 7911-12745

Figure 13

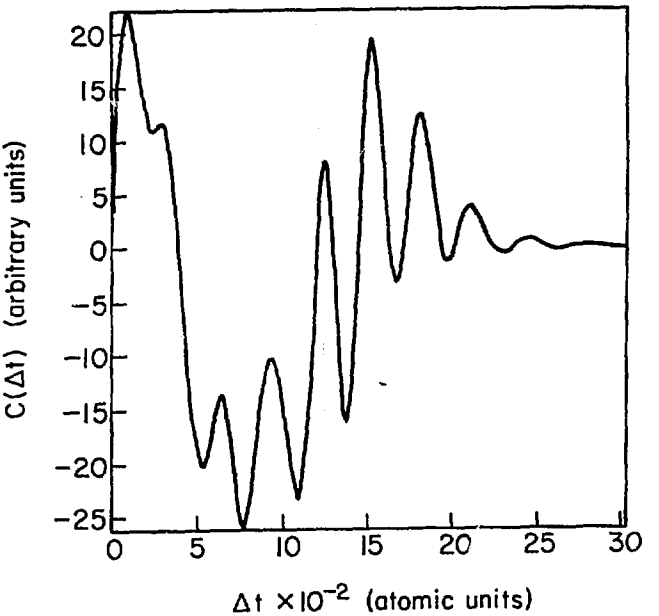

XBL 7911-12747

Figure 14

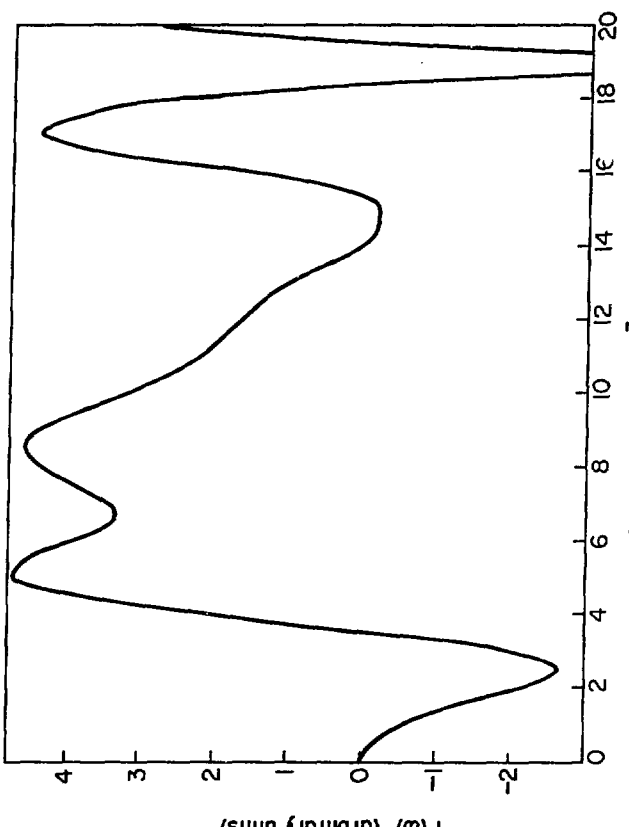

XBL 7911-12744

Figure 15

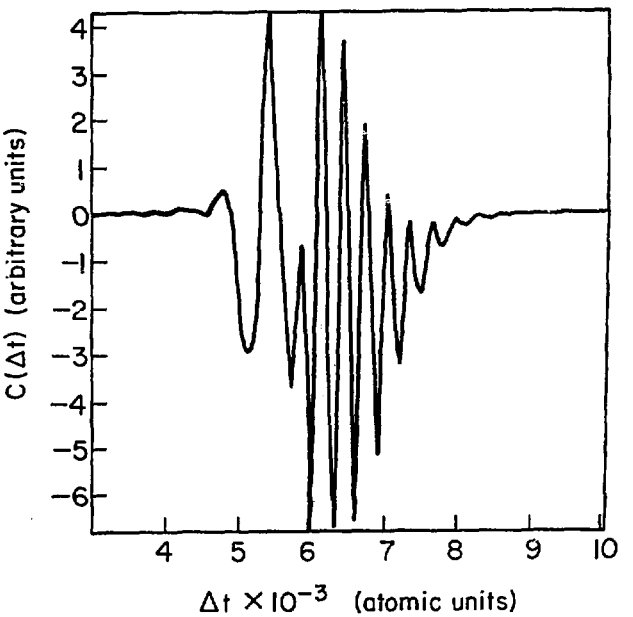

XBL 7911-12748

Figure 16

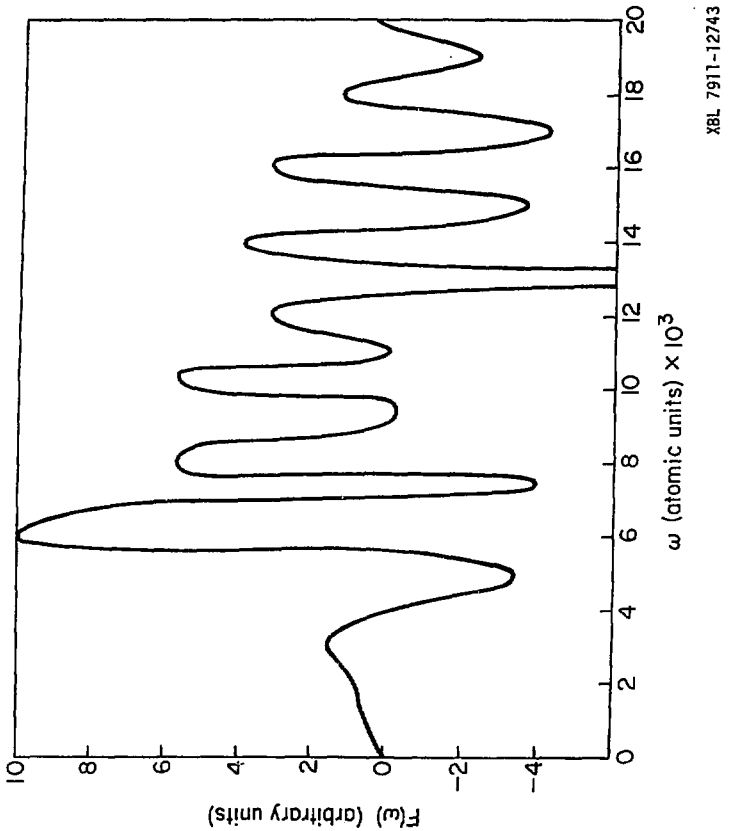

XBL 7911-12743

Figure 17

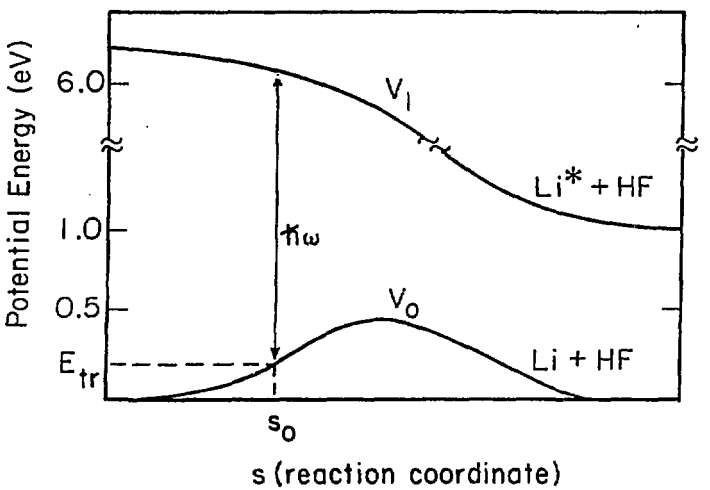

XBL 802-8043

Figure 18

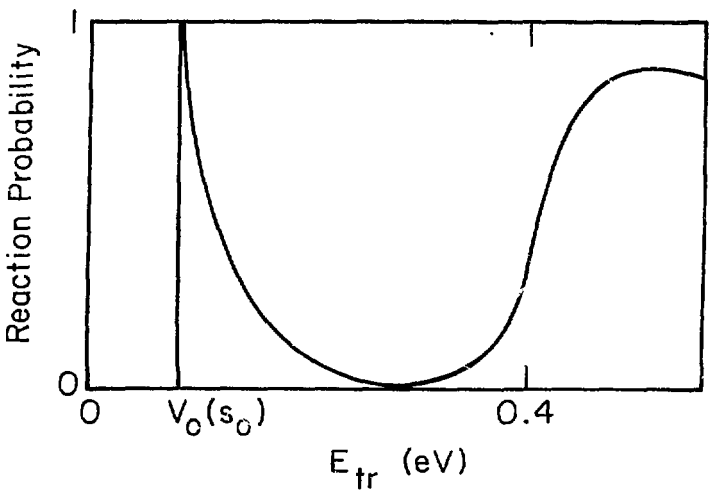

XBL 802-8044

Figure 19

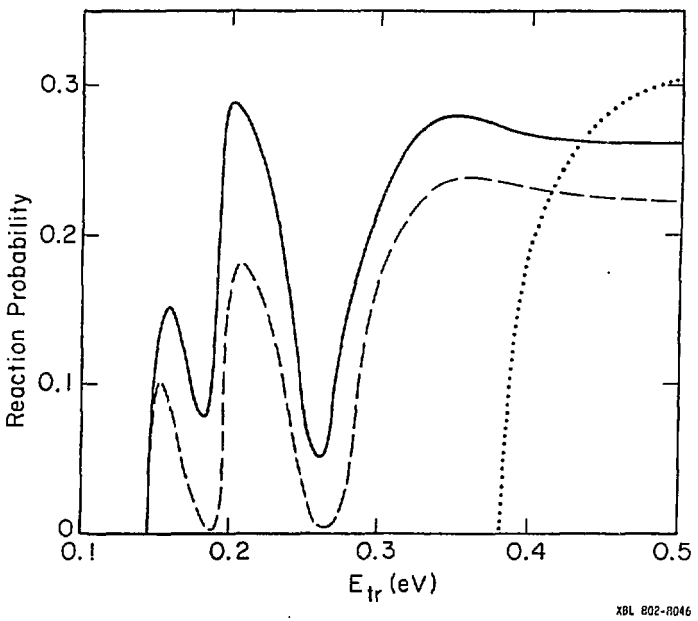
0.3
0.2
0.1
0
Reaction Probability
0.1
0.2
0.3
0.4
0.5
E_{tr} (eV)
XBL 802-A046

Figure 20

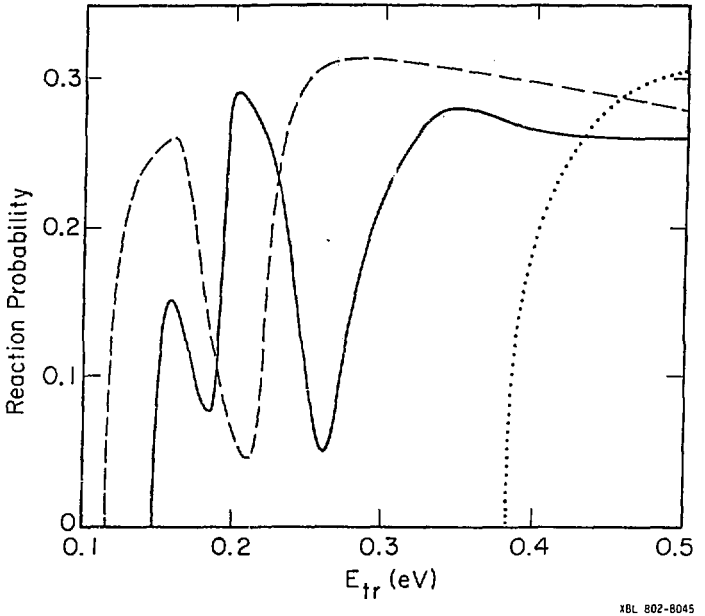
Reaction Probability
0.3
0.2
0.1
0
0.1
0.2
0.3
0.4
0.5
E_{tr} (eV)
XBL 802-8045

Figure 21

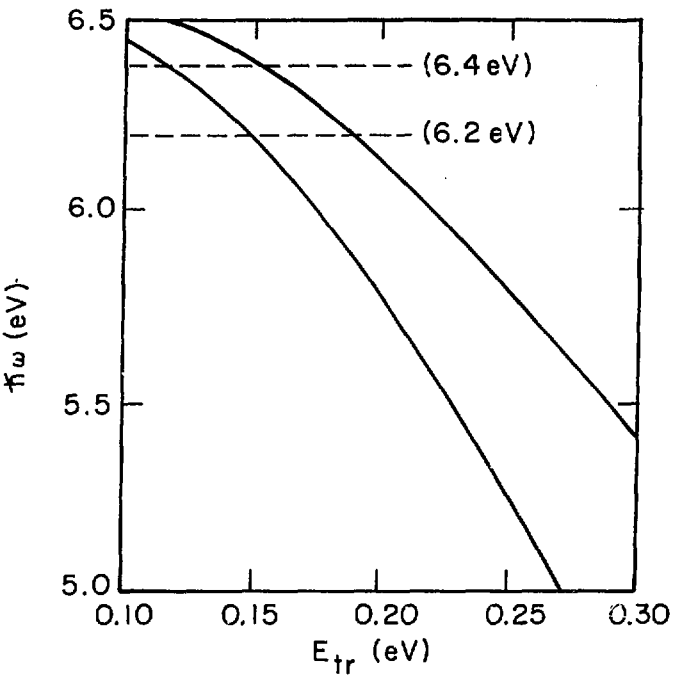

XBL 802-8130

Figure 22

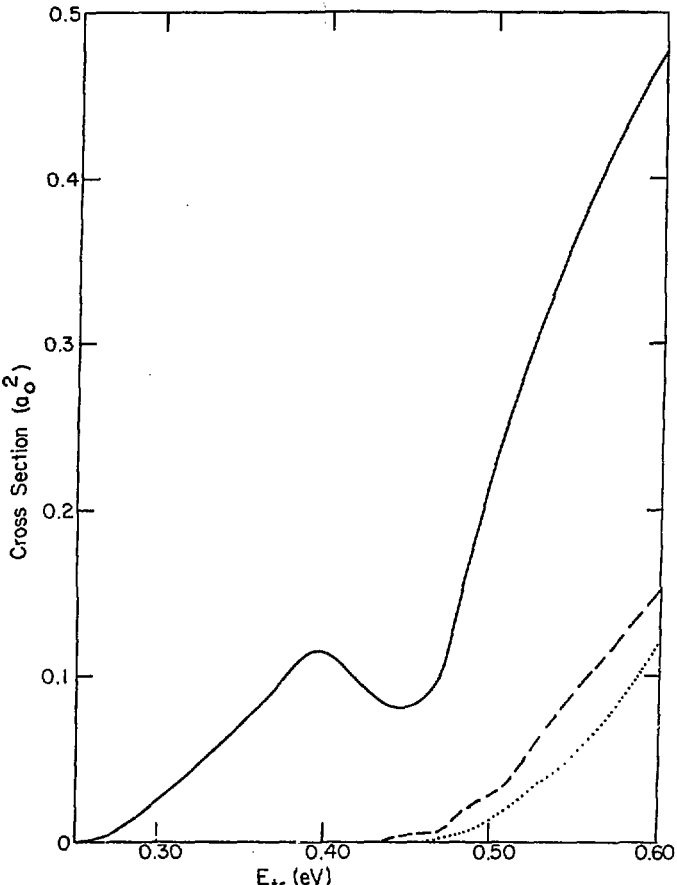
0.5
0.4
0.3
0.2
0.1
0
Cross Section (a_o^2)
0.30
0.40
0.50
0.60
E_{tr} (eV)
XBL 8010-12252

Figure 23

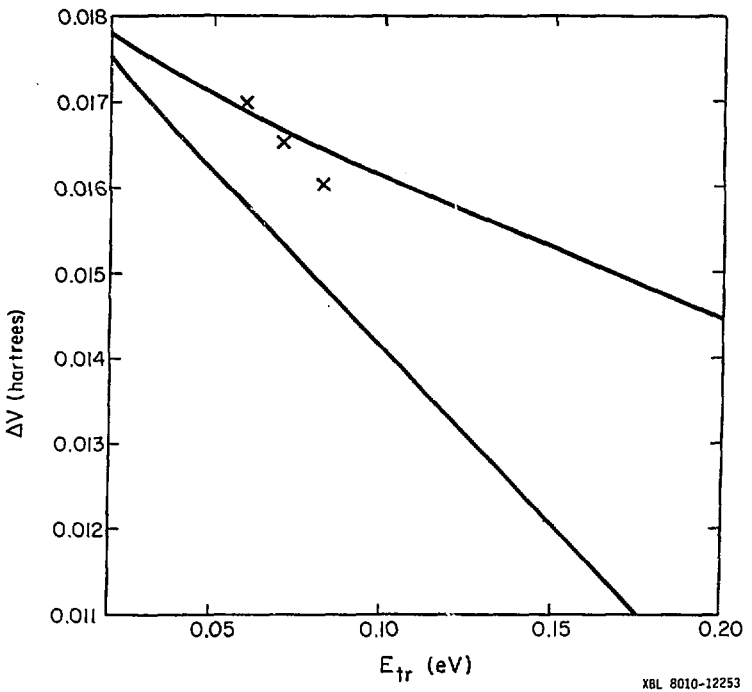
0.018
0.017
0.016
0.015
0.014
0.013
0.012
0.011
ΔV (hartrees)
0.05
0.10
0.15
0.20
E_tr (eV)
XBL 8010-12253

Figure 24

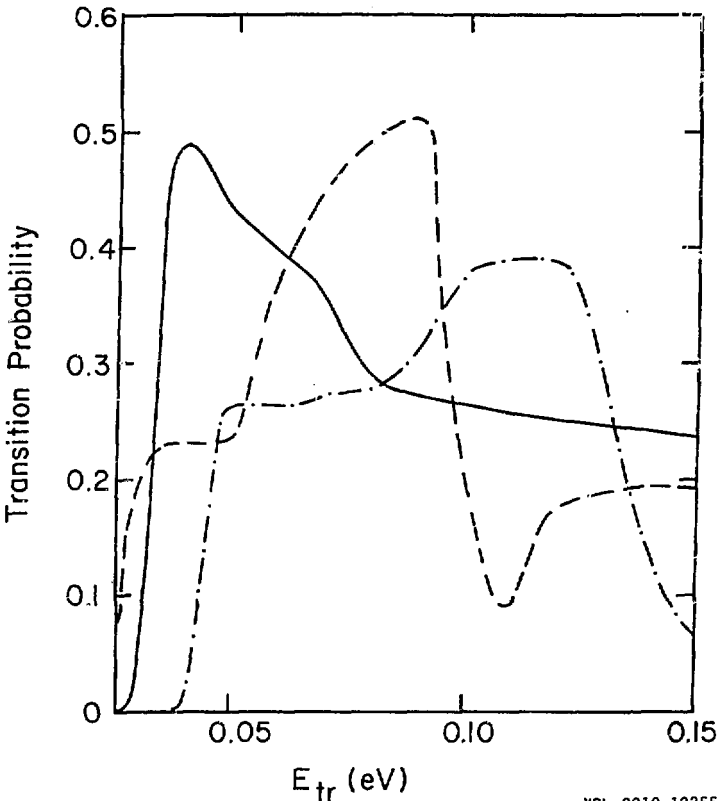
0.6
0.5
0.4
0.3
0.2
0.1
0
Transition Probability
0.05
0.10
0.15
E tr (eV)
XBL 8010-12255

Figure 25

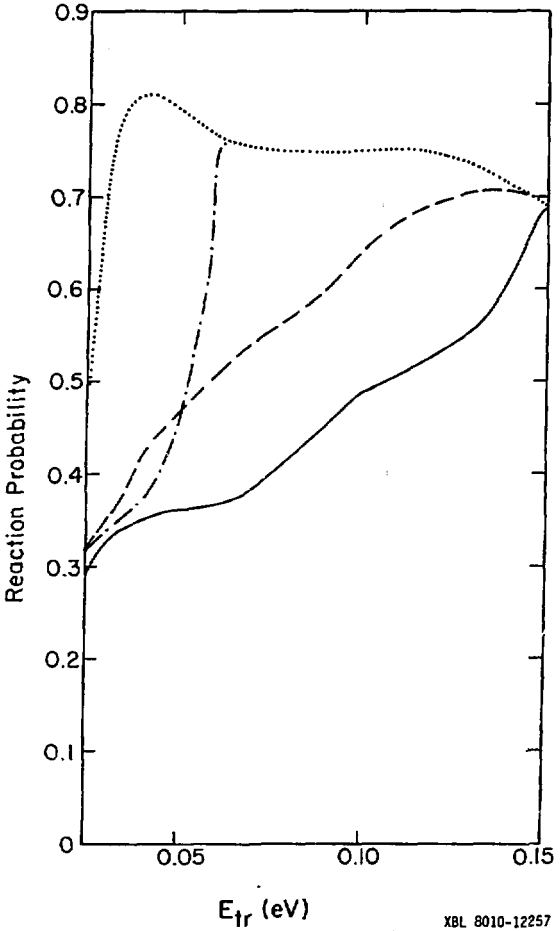
0.9
0.8
0.7
0.6
0.5
0.4
0.3
0.2
0.1
0
Reaction Probability
0.05
0.10
0.15
E_{tr} (eV)
XBL 8010-12257

Figure 26

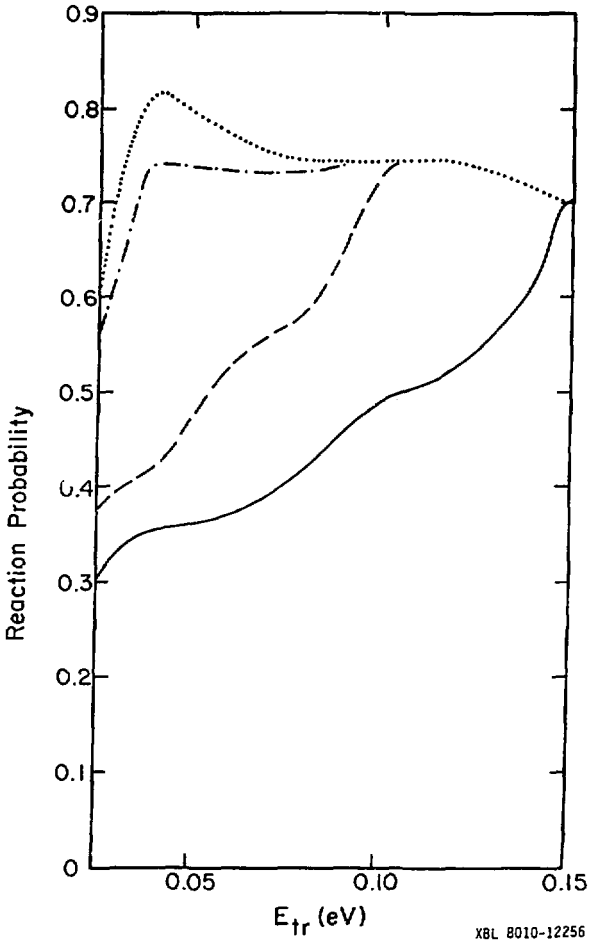
0.9
0.8
0.7
0.6
0.5
0.4
0.3
0.2
0.1
0
Reaction Probability
0.05
0.10
0.15
E_{tr} (eV)
XBL 8010-12256

Figure 27

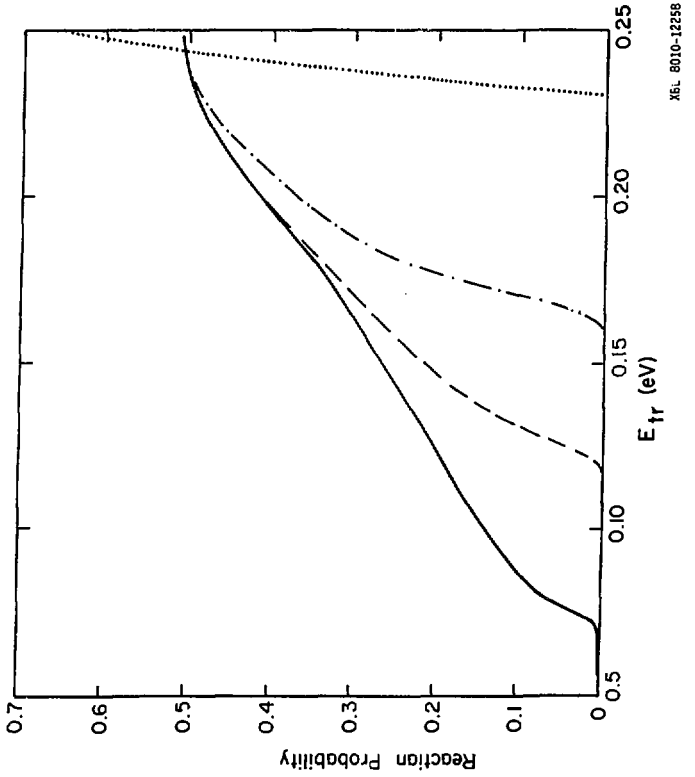
Reaction Probability
0.7
0.6
0.5
0.4
0.3
0.2
0.1
0
0.5
0.10
0.15
0.20
0.25
E_{tr} (eV)
XBL 8010-12258

Figure 28

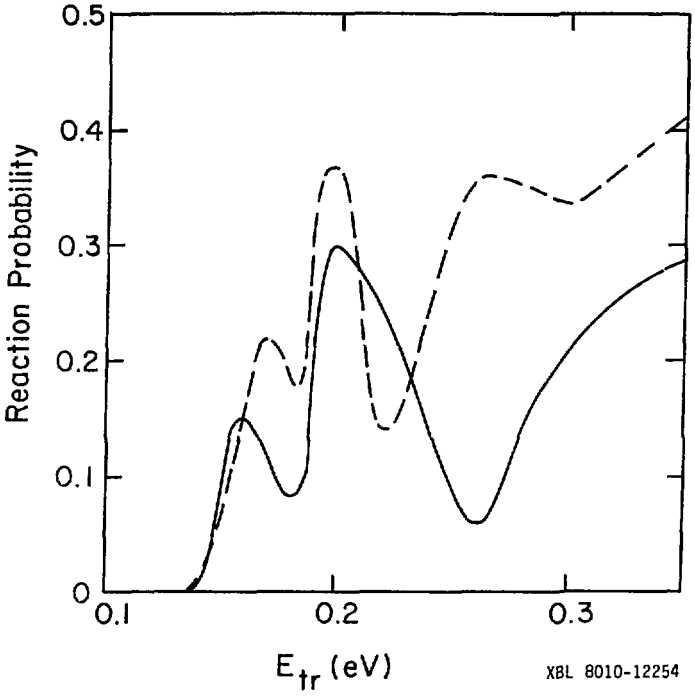
0.5
0.4
0.3
0.2
0.1
0
Reaction Probability
0.1
0.2
0.3
E_{tr} (eV)
XBL 8010-12254

Figure 29

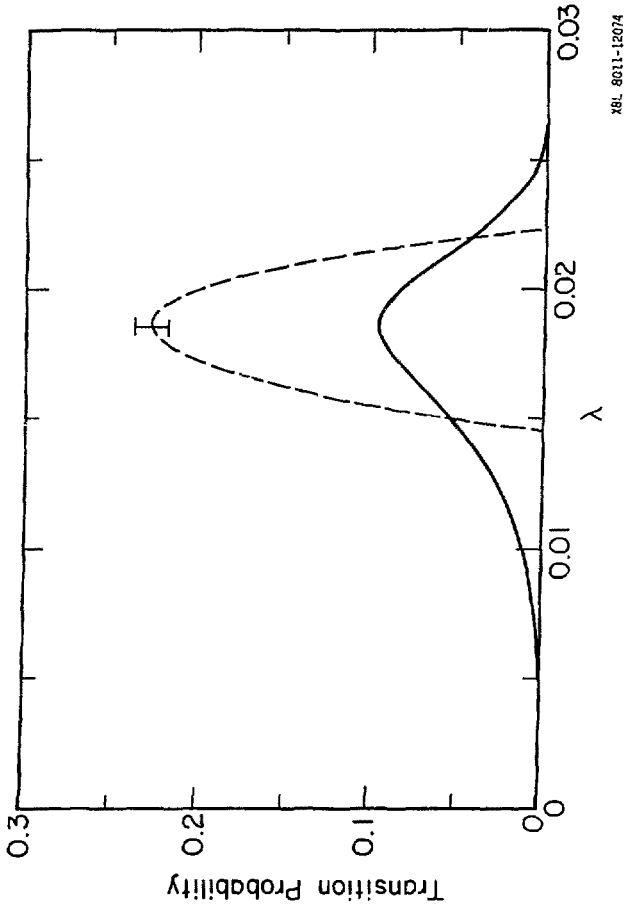
Transition Probability
0.3
0.2
0.1
0
0
0.01
0.02
0.03
λ
XBL 8011-12074

Figure 30

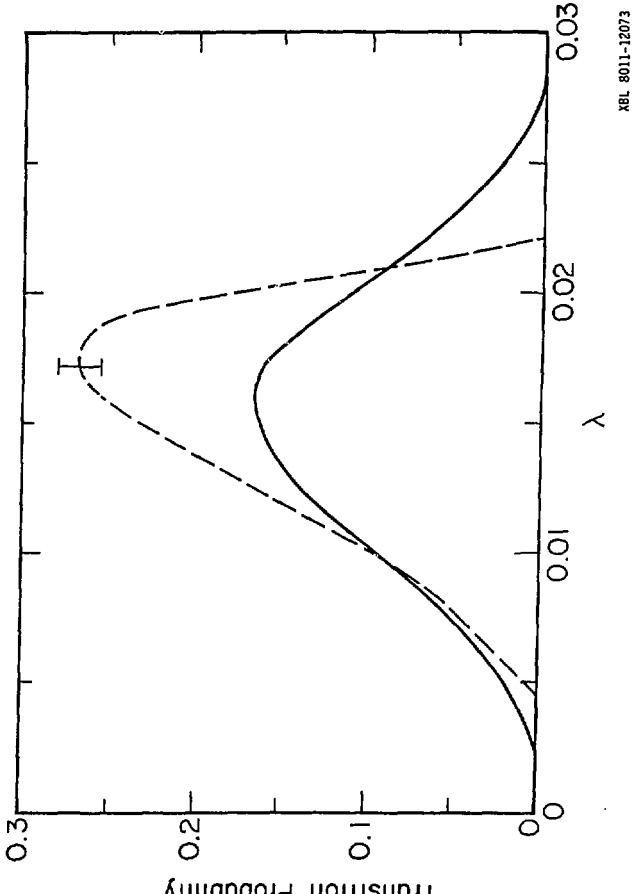
Transition Probability
0.3
0.2
0.1
0
0.01
0.02
0.03
λ
XBL 8011-12073

Figure 31

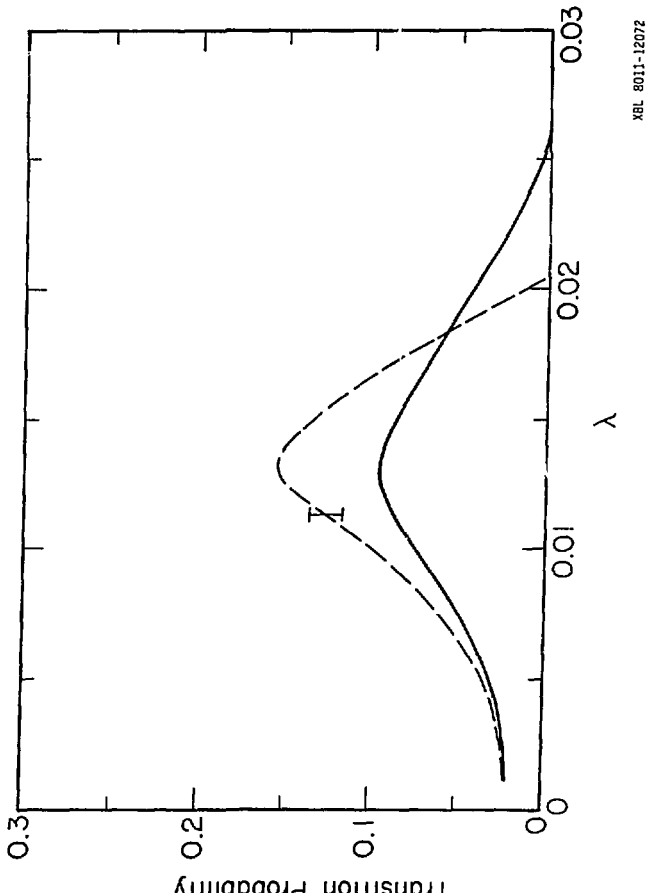
Transition Probability
0.3
0.2
0.1
0
0
0.01
0.02
0.03
λ
T
XBL 8011-12072

Figure 32